CHAPTER 1: INTRODUCTION

1.1 THE PERPETUATION OF THE BLUEPRINT FOR LIFE

The perpetuation of life depends on the ability of living cells to both sustain and replicate themselves. Cell division is a complex and highly regulated process whose purpose is to distribute exactly half of the duplicated genome into each daughter cell, and also to distribute the organelles and other cellular components evenly. This process can and, not infrequently, does go awry, resulting in an abnormal chromosome complement (aneuploidy) in the daughter cells. In humans, the effects of an abnormal number of chromosomes vary from a relatively mild disturbance of cellular function to lethality, with the vast majority of chromosomal variations not being compatible with life. At the level of the whole organism the most widely recognised chromosomal abnormality is Trisomy 21 or Down Syndrome, which results from an extra copy of chromosome 21. Exactly why Down Syndrome in particular is so common in humans remains elusive, as do the predominant cellular and molecular causes behind chromosome missegregation. This chapter introduces the human health consequences of aneuploidy and the current state of research knowledge of the underlying causes and cellular processes involved in cell division. This is followed by an in-depth look at key molecules underlying these processes, and finally a look at a model system to allow investigation of the molecular causes of chromosome missegregation.

1.2 HUMAN ANEUPLOIDY SYNDROMES

The phenomenon of chromosome missegregation is of considerable medical significance in terms of infertility and chromosomal abnormality disorders. Aneuploidy, an abnormal chromosome complement, arises through translocation of parts of chromosomes or missegregation of whole chromosomes during mitosis or meiosis. Aneuploidy arising in the gametes can lead to an aneuploid conceptus. In humans, the majority of aneuploid foetuses die *in utero* or, if full term is reached, suffer significant development defects and mental retardation. Despite the rigorous regulation of DNA replication and chromosome segregation at the cellular level, aneuploidy is a surprisingly common occurrence. An estimated 15-20% of all human oocytes are chromosomally abnormal, with 5% of all clinically recognised

pregnancies displaying aneuploidy (Hassold *et al.,* 2007). An estimated 57% of all spontaneous abortions in women under 35 years of age during the first trimester are due to chromosomal abnormalities, while this figure increases to greater than 80% in women over the age of 35 (Hogge *et al*., 2003; Hassold *et al*., 1980; Hassold *et al*., 1978). The vast majority of monosomies are lethal, with only monosomy of the X chromosome being compatible with life. Trisomies of some of the smaller chromosomes (eg 13, 15, 21, 22) can be viable, however, trisomic individuals suffer varying developmental issues.

The most common human trisomy leading to a live birth, trisomy 21 (T21 or Down Syndrome), is the leading cause of mental retardation in children, occurring in approximately 0.45% of human conceptions and between 1/319 and 1/1000 live births (Wiseman *et al*., 2009). Down Syndrome (T21), originally termed "mongolism" or "mongolian imbecility", was first described by John Langdon Haydon Down in 1866. As early as 1909 a link between birth order and Down Syndrome had been observed, which led to the suggestion that children born later to an older mother were more likely to suffer Down Syndrome (Shuttleworth, 1909). From the 1930s several theories of a maternal age effect based on surveys and statistical analysis were suggested (Penrose, 1934; Smith and Record, 1955). In 1959 Lejeune and Jacobs *et al*. determined the karyotypic abnormality underlying Down Syndrome, most commonly an extra copy of the small acrocentric chromosome 21.

For half a century links between maternal age, meiotic recombination, meiotic missegregation events and aneuploidy have been recognised, but until recently, surprisingly little progress had been made towards determining the molecular mechanisms for meiotic aneuploidy. What is known is that two distinct mechanisms exist: non-disjunction (ND), where chromosomes or chromatids fail to separate and precocious division (PD), where chromosomes or chromatids separate prior to anaphase (Angell, 1991). In meiosis I (MI) ND results in the loss or gain of a whole extra chromosome, while PD results in gain or loss of a single chromatid (Rosenbusch, 2006; Pellestor *et al*., 2002). The majority of evidence gathered through DNA polymorphism and cytogenetic studies looking at the origin, recombination rates and sites of recombination along the extra chromosome in T21

concluded that the majority of missegregation occurs during MI from non-disjunction of bivalents (Valle *et al*., 2006; Perroni *et al*., 1990; Stewart *et al*., 1988; Hamers *et al.*, 1987; Warren *et al*., 1987). In contrast, studies using direct karyotype analysis of unfertilised oocytes and their polar bodies indicate that PD has been underestimated as a source of aneuploidy, most likely because earlier studies assumed ND as the sole mechanism and scored single chromatids as whole chromosomes (Pellestor *et al*., 2002; Angell, 1997). Kuliev *et al*. (2004) found that single chromatids represented the majority of MI abnormalities, indicating a higher rate of PD over ND. This study also indicated that MI errors are likely to occur only slightly more frequently than MII errors, however, randomly segregating extra chromatids appear to be directed to the polar bodies and therefore MII errors are more frequently nullified and under-represented in conceptions.

Recurrence of T21 in subsequent pregnancies is higher in younger mothers, but the incidence of T21 generally is higher in older mothers, with recent evidence suggestive of different pathways for reaching T21 (Hulten *et al*., 2008; Hassold and Hunt, 2008; Oliver *et al*., 2008). The exact circumstances that lead to cells failing to segregate all their chromosomes correctly remain unclear. However, many genetic, cellular and environmental factors are likely to contribute, as discussed below.

1.2.1 Current theories on the origins of female meiotic aneuploidy

1.2.1.1 Gender- and species-specific susceptibility

Compelling evidence from trisomy and polar body chromosome analyses suggests that, when compared to human spermatogenesis, or oogenesis in other mamamalian species, human oogenesis is acutely susceptible to chromosome segregation errors (Pacchierotti *et al*., 2007; Fragouli *et al.*, 2006). Studies mapping the origin of the extra chromosomes indicate that ~90% of T21 cases are of maternal origin, while ~10% are of paternal origin (Hassold and Hunt, 2001). Although a maternal age effect has also been demonstrated in mouse models, the effect is an order of magnitude lower than that observed in human females. Such a dramatic difference in error rates between spermatogenesis and oogenesis is less surprising as these are quite distinct developmental processes and with significant divergence of the

regulatory mechanisms and pathways through evolution. Oogenesis in mammals, on the other hand, is mechanistically very similar between species in terms of the development of oocytes during embryogenesis, the presence of a prolonged meiotic arrest, as well as conservation of key cell cycle checkpoints and regulatory pathways. Why the error rate in humans is atypical, among mammals, is presently unknown. It may be indicative of unique environmental influences specific to humans, or of unidentified environmental, genetic or structural factors in some human chromosomes that can influence their heritability and continuance in the human genome pool.

1.2.1.2 Old oocytes

Spermatogenesis and oogenesis have quite distinct spindle requirements as spermatogenesis involves two equal divisions resulting in four haploid gametes, whereas oogenesis involves two asymmetrical cytokinesis events to produce a single gamete and two polar bodies that contain the discarded chromosomes. In male humans, meiosis commences when sperm production is required at the onset of puberty and sperm are produced continuously throughout the lifetime of a man, albeit with some decline in quality over time. In stark contrast, oocytes commence the journey through meiosis when a female is *in utero*. Oocytes undergo prolonged cell cycle arrest and only complete the first meiotic division when the oocyte is released during ovulation sometime after the onset of puberty. This phenomenon of pausing meiosis for an extended period of time and observations of a severe decline in oocyte "fitness" after 35 years of age (the maternal age effect) has led many to hypothesise that as women age, oocyte cell cycle checkpoint control becomes less stringent and/or cellular repair mechanisms become less efficient, resulting in an explosive increase in genetically flawed oocytes being ovulated. In women aged 20 years the risk of a T21 birth is 1/1,667, rising to 1/378 at the age of 35 and 1/11 at the age 49 (ASRM, 2003). This age-dependent risk of aneuploidy also applies to other chromosomes and the risk of spontaneous abortions increases dramatically after the age of 35 (ASRM, 2003). It remains a point of debate as to whether errors arise because the repair and monitoring systems have declined or whether the remaining oocyte population, when approaching menopause, consists of a higher proportion of poorer quality oocytes that the body is prepared to risk ovulating as a response to the evolutionary consequences of not reproducing.

1.2.1.3 Altered recombination

Recombination, where homologous chromosomes undergo exchange of genetic material, is an integral feature of meiosis, with normally at least one recombination site per chromosome. Chiasmata, the physical sites of crossovers between recombined chromosomes, are essential for meiotic chromosome cohesion and accurate chromosome segregation. The number of crossovers per chromosome is proportional to chromosome length, while the probability of missegregation is inversely proportional to the number of crossovers and chromosome length. Hence, small chromosomes (eg. human chromosome 21) suffer a relatively high degree of missegregation. Investigations into the recombination rates between chromosomes that have resulted in trisomy 21 have revealed that 45% of these chromosomes were achiasmate (no recombination sites), compared to 0% of correctly segregated chromosomes 21 (Oliver *et al*., 2008; Lamb *et al*., 1997). The sites of recombination events have also been found to correlate with risk of T21, with 40% of investigated T21 chromosomes having a single recombination site at the distal end of 21q and 29% of investigated T21 chromosomes having a single recombination site at the proximal end of 21q, compared to normally segregation chromosomes 21 which had 56% of single crossovers at a median 21q position (Oliver *et al*., 2008; Lamb *et al*., 1997).

Robles *et al.* (2009) have demonstrated that the number and positioning of recombination sites are quite different between spermatocytes and oocytes, possibly linking recombination with the sex-specific difference in T21 origin. It is not unusual in humans for small chromosomes to have only a single recombination event; however, the positioning of the crossover can be crucial (Robles *et al*., 2009). When a homologous chromosome pair carry a single crossover positioned close to the telomeres, the chiasma may not be sufficient to physically resist the tension of the mitotic spindle causing premature bivalent separation. This telomeric crossover characteristic is more commonly associated with T21 cases occurring with young mothers. Conversely, chiasmata located in the pericentromeric region can also induce missegregation events, a characteristic more prevalent in MII-derived T21 cases associated with older women. It is now widely recognised that a subset of MII missegregation events are associated with pericentromeric recombination events that arise during MI and only resolve in MII, therefore these cannot be considered to be

arising through a unique MII mechanism (Sherman *et al*., 2006; Hassold *et al.*, 2000; Hassold and Sherman, 2000). T21 cases associated with achiasmate chromosome have been identified as equally common between younger and older mothers and no evidence of a change in exchange rate is observed with increasing age (Oliver *et al.*, 2008; Lamb *et al*., 2005; Sherman *et al*., 2006). In younger women susceptible recombination configurations (i.e. pericentromeric or telomeric positioning of chiasmata) appear to be a leading risk factor for chromosome 21 MI missegregation, while in older women MI missegregation frequently occurs with chromosomes that have non-susceptible recombination configurations (Sherman *et al.*, 2006). This is suggestive of a general decline in the meiosis machinery fidelity with age.

The original studies into the origin of the extra chromosome in T21 developed the theory that if the two copies of a maternal (or paternal) chromosome 21 were heterozygous at the centromeric region then non-disjunction must have occurred during MI (Figure 1.1). By this logic, chromosomes with homozygous centromeric regions must have non-disjoined during MII. These analyses worked on the assumption that the MI bivalents undergo non-disjunction, resulting in an extra bivalent at MII and that both products of the MII division will each carry an extra chromosome. In contrast, studies using MII arrested oocytes from assisted reproduction programs have identified single extra chromosomes at MII as well as the predicted extra bivalent chromosome pair (Fragouli *et al*., 2006; Mahmood *et al.*, 2000; Angell, 1997; Dailey *et al*., 1996; Angell *et al*., 1994; Angell *et al*., 1991). This clearly demonstrates an alternative mechanism for aneuploidy to occur and indicates that non-disjunction may not in fact be the main mechanism for trisomy, but that premature separation of the kinetochores could drive chromatids to act as univalents with the inheritance pattern being determined by the placement of crossovers. It is also predicted that the more distal a crossover, the more likely that chromatids rather than homologues will separate at the first meiotic division if bivalents have undergone PD (Figure 1.1) (Wolstenholme and Angell, 2000; Angell, 1997). While this situation may resolve into a normal chromosome complement, issues arise if the chromatids segregate randomly in MI and raises questions about theories arising from studies that assumed MI or MII origin based on centromeric homology.

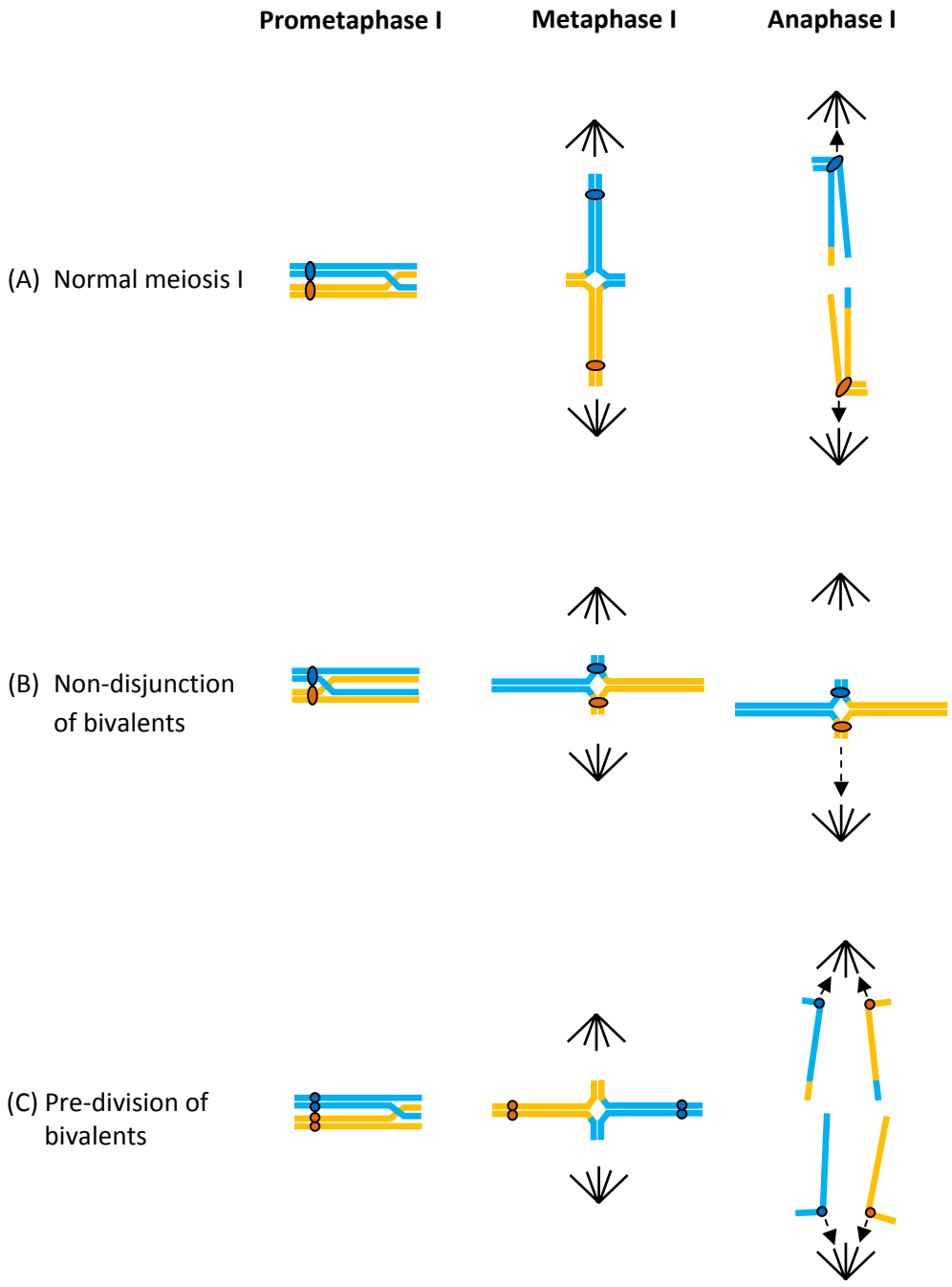

Figure 1.1: Possible meiosis I chromosome configurations. (A) Normal meiosis I: homologous chromosomes synapse and segregate away from each other. (B) Non-disjunction of homologues: the bivalents fail to resolve into univalents and consequently missegregate to the same pole. (C) Pre-division of bivalents: cohesion is lost between homologues and chromatids; the remaining distal crossover directs the chromatids to segregate rather than the homologues.

1.2.1.4 Meiotic drive

Maternal age currently remains the major correlated risk factor for aneuploid conceptions. This phenomenon is mathematically predicted by the Meioitic Drive (MD) theory (Day and Taylor, 1998; Malik and Bayes, 2006), which assumes that homologous chromosomes are driven to divide towards the ovum and away from the polar body. Based on the asymmetric nature of female meiosis, the theory predicts that females will be affected during MI, as this is when the greatest selective pressure is applied as one homologue in a pair segregates to the ovum while the other segregates to the polar body with no hope of contributing to the next generation. The mathematical models predict the exponential increase in trisomic conceptions that is observed in human females over the age of 35 years. An explanation for this phenomenon is that as menopause, the finalé for chromosomal inheritance from females, is approaching, meiotic drive exceeds the control measures in place to prevent aneuploidy (Day and Taylor, 2006). The MD theory only predicts the outcome of selective pressure on chromosome segregation and does not indicate any molecular mechanism by which this may come to pass. However, various examples exist of chromosomes that contain selfish DNA elements that enable preferential inheritance, such as increased microtubule binding sites at the centromere (Presgraves *et al*., 2009; Palestis *et al.*, 2004; Henikoff and Malik, 2002).

1.2.1.5 Grandmaternal effect

Recent research has implicated grandmaternal age as a significant contributor to risk of T21 conceptions in daughters (Malini and Ramachandra, 2006). In contrast to western studies that have previously demonstrated strongest correlation with maternal age, pedigrees in larger Indian families demonstrate an extremely strong association between grandmaternal age when daughters were conceived and T21 grandchildren. Of the 69 T21 cases investigated, 52 were born of women aged 18-29 years, whereas in 61 of these cases the grandmothers were aged 30-40 years when they had conceived the mothers (Malini and Ramachandra, 2006). Although there is currently little in the way of other studies that support these findings, this evidence raises interesting questions as to the molecular mechanisms by which chromosomes mis-segregate to result in T21 conceptions. The most plausible molecular explanation for the grandmaternal effect involves epigenetic mechanisms

and may indicate that reduced recombination rates are not maternal-age dependent, but arise from much earlier events during development when grandmaternal epigenetic influences alter recombination events *in utero*.

1.2.1.6 Ovarian mosaicism

In contrast to the historic wisdom that the majority of trisomies result from primary non-disjunction of homologues during MI, there is evidence to support a theory that many human females are actually trisomy 21 ovarian mosaics (Hulten *et al*., 2008; Sachs *et al.*, 2004; Tseng *et al*., 1994). In the Hulten study every ovary analysed from eight developmentally normal foetuses (aborted for social reasons) was an ovarian mosaic, however, only 0.2-0.88% of cells analysed were T21. This is unlikely to explain the high recurrence rates of T21 observed in some women, however, studies involving women with recurrent T21 conceptions identified T21 cells in the small population of cells from ovarian biopsies and ovulated oocytes, indicating that in some women the number of T21 cells in the ovaries is likely to be much higher than 0.2-0.88% (Sachs *et al.*, 2004; Tseng *et al*., 1994; Nielsen *et al*., 1988; Parke *et al*., 1980). High penetrance of ovarian mosaicism in the human population potentially provides a new explanation for the observed maternal age effect, as T21 oocytes have been found to develop more slowly and may be ovulated much later (Hulten *et al*., 2008). Hulten *et al*. (2008) have also suggested that the altered recombination rates and positions observed in T21 chromosome studies can be explained by the presence of an extra chromosome 21 and secondary non-disjunction when the cells divide. Cell division with an extra homologue has been shown to result in a bivalent and an achiasmatic univalent or a trivalent (Barlow *et al.*, 2002; Luciani *et al*., 1976) that are predicted to force recombination events in proximal or distal positions. Although many aspects of this theory are compelling, it is currently unclear how this mosaicism would arise.

1.2.1.7 Aneugens and environmental effects

Many chemicals and other environmental factors have been implicated in increasing aneuploidy (Table 1.2). Much of these data, however, comes from unreplicated small-scale studies. Further evidence of effects on both sexes, replication in other species and investigation of molecular mechanisms is clearly required. Some investigations into environmental factors have proved intriguing but inconclusive; this is most likely due to study design and assumptions employed. Study design is extremely complex when considering which stage of meiosis may be relevant to exposure, particularly in females where MI commences in the foetus and completes at ovulation some 10-50 years later, and the synergistic effects of some chemicals (Yang *et al*., 1999). Intracellular environmental factors that influence spindle-forming ability or cell cycle progression have also been proposed as potential aneugens. Van Blerkom (1996) demonstrated a link between reduced cellular pH, impaired spindle formation and aneuploidy in aging oocytes. This situation has been hypothesised for aging follicles where a hormone imbalance results in compromised microcirculation, leading to increased intracellular CO_2 and decreased pH (Gaulden, 1992).

Table 1.1: Known aneugens

Lifestyle factors	Cigarette smoking	Wyrobek *et al*., 1993; Robbins *et al.*, 1997b, 2003; Shi *et al.*, 2001)
	Alcohol	(Robbins *et al.*, 1997b)
	Caffeine	(Robbins *et al.*, 1997b)
Radiation	Ionising radiation	(reviewed in Verger, 1997)
Medications	Chemotherapy	(Monteil *et al.*, 1997; Robbins 1997a; Martin *et al.*, 1995, 1997, 1999; De Mas *et al.*, 2001; Frias *et al.*, 2003)
	Diazepam	(Baumgartner *et al.*, 2001)
	Oral contraceptive	(Yang *et al.*, 1999)
Chemicals	Acrylonitrile	(Xu *et al.*, 2003)
	Bisphenol-A (BPA)	Hunt *et al*., 2003; Susiarjo *et al*., 2007
Pesticides	Trichlorfon	(Czeizel *et al*., 1993)
	Other	(Padungtod *et al*., 1999; Xia *et al*., 2004; Recio *et al*., 2001; Smith *et al*., 2004)

1.2.1.8 Molecular mechanisms

Despite over 100 years of research into the causes of T21 and aneuploidy, much remains unknown of the pathways, and the exact factors underpinning these pathways, that lead to chromosome missegregation. The majority of hypotheses for molecular mechanisms by which aneuploidy arises during meiosis are drawn from the evidence of sex-specific rates of aneuploidy, the maternal age correlation, reduced recombination rates and chemical inducers of aneuploidy. A key figure in the hypothesised molecular mechanisms is the meiotic spindle, as it is central to accurate chromosome segregation and provides the basis for a molecular checkpoint in the cell cycle. Failure of the spindle assembly checkpoint (SAC) to halt cells that have unattached chromosomes would severely disrupt the fidelity of chromosome segregation and produce aneuploid cells (Vogt *et al*., 2008). Meiotic recombination is also a key factor in the development of aneuploidy. As discussed in section 1.2.1.3, recombination rates and the positioning of recombination events both correlate strongly with risk of chromosome 21 missegregation. Despite the strong evidence linking recombination rates with aneuploidy, the mechanisms by which recombination events are altered are still very vague. It is also becoming clear that aneuploidy arising at different points within meiosis can have quite different aetiology.

1.3 ACCURATE CHROMOSOME SEGREGATION

Missegregation of chromosomes is highly deleterious as it results in an abnormal chromosome number (aneuploidy), disrupting the delicate balances of gene dosage, regulatory networks and homeostatic processes that normally exist in a diploid cell. Aneuploid yeast cells have been demonstrated to have cell cycle progression defects, increased glucose uptake and increased sensitivity to conditions interfering with protein synthesis and folding, generally putting them at a proliferative disadvantage (Torres *et al*., 2007). The deterimental effects of altered gene dosage have also been observed in *Drosophila* and human trisomy 21 fibroblast cell cultures (Lindsley *et al.*, 1972; Segal and McCoy, 1974). Studies in plants have shown that aneuploidy is much more deleterious than polyploidy (whole genome duplication) due to the imbalances generated in the stoichiometry of multi-protein complexes and other dosage-sensitive relationships (Birchler and Veitia, 2007).

1.3.1 The cell cycle and checkpoints

Integral to the chromosome segregation process are the cell cycle restriction points and checkpoint pathways. Entry into the cell cycle (Figure 1.2) is restricted in G1 in response to nutrient availability, cell size, contact inhibition and other external signals (G1 restriction point). Cell-cycle checkpoints ensure that any DNA damage is repaired prior to DNA replication or cell division (DNA damage checkpoints G1-S and G2-M), that chromosomes are fully replicated only once in a single round of cell division (G2-M checkpoint), and chromosomes are correctly aligned on the metaphase spindle (spindle assembly checkpoint, SAC) (Figure 1.2). The DNA replication checkpoint and SAC function at very restricted points in the cell cycle, halting the S-G2 and metaphase-anaphase transitions, respectively. While the DNA damage checkpoint is activated in G1, it can halt cell cycle progression in the G1 or G2 phases and slow down S phase while repair genes are upregulated (Elledge, 1996; Nasmyth, 1996; Vogt *et al*., 2007; Lukas *et al.*, 2004). Checkpoint-arrested cells that cannot repair damage, or correct replication or spindle errors, can be eliminated by apoptosis, a cell death pathway which removes abnormal cells from the body.

The SAC regulates the metaphase-anaphase transition, preventing precocious sister-chromatid separation. The SAC specifically targets the APC-C through the effector complex, mitotic checkpoint complex (MCC), made up for MAD2, BUBR1, BUB3 and the APC-C regulatory subunit CDC20 (Sudakin *et al*., 2001; Shannon *et al*., 2002; Poddar *et al*., 2005). Many other proteins are considered as core components of the SAC pathway, including BUB1, MAD3, MPS1 and AURORA-B, or are recognised regulators of the SAC pathway, including ROD, ZW-10, ZWILCH, PLK1, CDK1-cyclin B (Musacchio and Salmon, 2007; Karess *et al*., 2005; van Vugt and Medema, 2005; D'Angiolella *et al*., 2003; Kallio *et al*., 2002). The proteins of the SAC have been demonstrated to accumulate at the kinetochores of chromosomes that are unattached by spindle microtubules at metaphase. These proteins disperse once microtubules attach, providing a monitoring system for the orientation of chromosomes and establishment of tension across the metaphase plate (Chen *et al*., 1998; Taylor *et al*., 1998; Rieder *et al*., 1995; Rieder *et al*., 1994). Once the chromosomes are correctly oriented the SAC becomes inactivated, this allows activation of the APC-C, which marks Cyclin B and Securin for degradation, driving on the onset of anaphase (Musacchio and Salmon, 2007; Hagting *et al*., 2002; Clute and Pines, 1999). Securin is the stoichiometric inhibitor of Separase, the protease that proteolytically cleaves the cohesin complex and allows chromosomes to segregate.

The fidelity of the meiotic spindle has been identified as a pivotal player in the maternal age effect. The asymmetry of the oogenesis divisions underlies the higher observed susceptibility female gametogenesis to cytoskeletal abnormalities (Pacchierotti *et al*., 2007; Shin and Choi, 2004). A sex-specific weakening of the SAC has also been suggested as the potential key to the maternal age effect. These hypotheses are supported by evidence of chemical induction of aneuploidy in MI of rodents using microtubule damaging agents, including colchicine, griseofulvin, taxol, vinblastine and benomyl (Swanton *et al*., 2009; Salmon *et al*., 1984; Sloboda *et al*., 1982; De Brabander *et al*., 1986; Jordan and Wilson, 1998), which increased the frequency of aneuploidy in rodent MII oocytes from a baseline of 0.5-1.0% to 23-42% (Mailhes *et al*., 1990, 1993a, 1993b, 1999; Russo and Pacchierotti, 1988; Mailhes and Aardema, 1992).

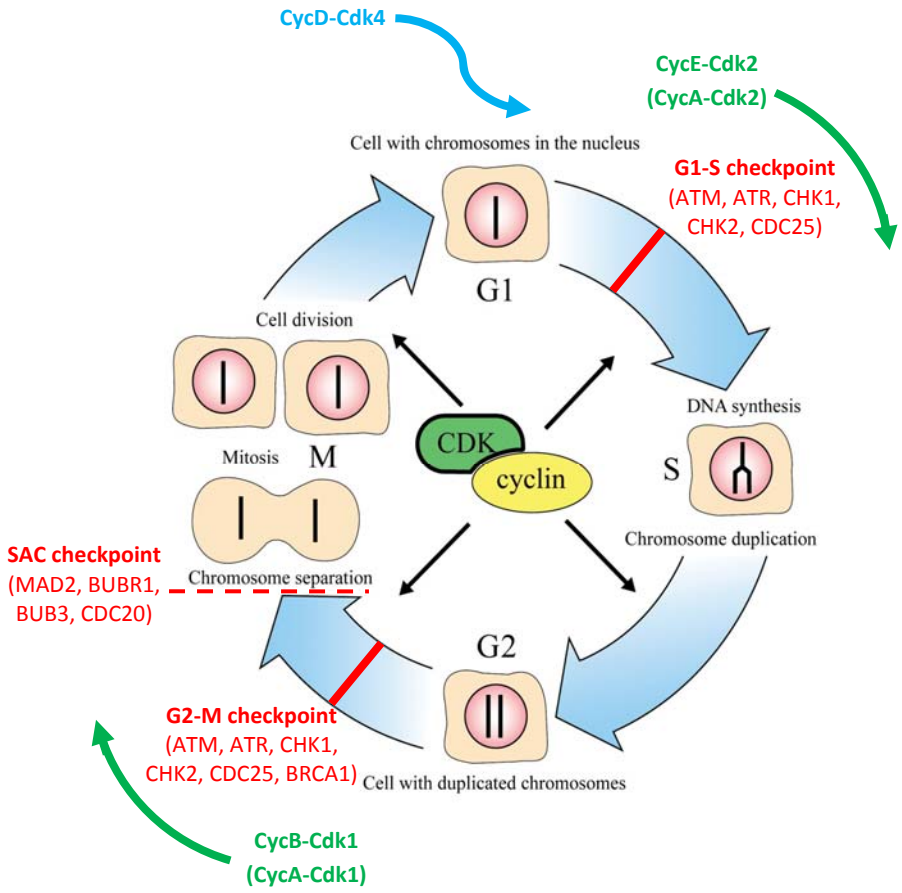

Figure 1.2: The cell cycle and checkpoints. A cell that is signalled to replicate passes a restriction point in gap phase 1 (G1), from which point the cell accumulates mass and nutrients and is committed to divide. When sufficient resources have been acquired the cell enters the synthesis phase (S), when the entire genome is replicated once. Following on from replication the cell enters gap phase 2 (G2), when errors or damage that occurred during the replication process are detected and repaired. During the growth phases the organelles and lipid membranes must also be replicated and enlarged in preparation for cell division, which occurs directly following M phase when the replicated genome is divided exactly in half. Specific cyclin-CDK partners are responsible for controlling the entry and exit from each phase of the cell cycle.

1.3.2 Chromosome cohesion and recombination

Cohesin (discussed in detail in section 1.4) is a protein complex that facilitates chromatid cohesion and is essential for maintaining the chiasmata that link homologous chromosomes (Kudo *et al*., 2009; Kudo *et al*., 2006; Buonomo *et al*., 2000; Van Heemst and Heyting, 2000). Mice lacking SMC1β, a meiosis-specific cohesin subunit demonstrate an age-dependent increase in aneuploid conceptions and births closely resembling the age-dependent increase observed in the general human population (Hodges *et al.*, 2005). This is supported by a *Drosophila* model where a reduction in SMC1 levels induces a concomitant increase in recombinant homologue missegregation as the flies' age (Subramanian and Bickel, 2008). These models indicate that a lack of cohesin to maintain chiasmata is tolerable in young females with young oocytes, where other cellular processes are able to compensate. Cohesin is an essential feature of chiasmata, preventing the crossovers "sliding off" the end of the chromosome and being lost. A decline in chiasmata frequency with increasing age was first observed in mouse oocytes by Henderson and Edwards (1968). More recent studies have shown that, although the original sites of recombination can be detected in gametes using MLH1 antibodies that localise specifically to recombination foci, analysis of the physical crossovers frequently reveals both distal "slippage" of the chiasmata or complete loss of chiasmata in the absence of SMC1β containing cohesin complexes (Hodges *et al*., 2005). Once all chiasmata linking bivalents are lost, nothing remains to hold the chromosome pairs together and they are able to randomly segregate. Therefore, loss of cohesin from chromosomes with increasing age is a potential suspect that could explain the frequent loss of genomic integrity with increasing maternal age. However, if or how cohesin is lost from meiotic chromosomes is presently unknown.

The observed decrease in chiasmata number with age has led some scientists to hypothesise that the functionality of the proteins holding chromosomes together, which are originally loaded in S phase prior to MI arrest, may decline as the proteins age. There is little in the way of direct evidence to suggest that the same protein molecules are maintained from foetus to adulthood. Instead, experiments from several groups have demonstrated that chromosome-bound cohesin complexes are highly dynamic and undergo frequent exchange during a cell cycle without affecting chromosome cohesion (McNairn and Gerton, 2009; Gerlich *et al*., 2006). Other

research groups have demonstrated global loading of cohesin in response to DNA damage following replication, indicating that there are potential mechanisms within cells by which proteins holding the chromosome together can be replaced. Therefore, it would seem plausible that, with increasing age, there is a general decline in the efficiency and stringency of all pathways leading to accurate chromosome cohesion and segregation.

The close resemblance of the mouse SMC1β and the *Drosophila* SMC1 models to the human maternal age effect is very suggestive of the cohesin complex playing a central role in the maternal age effect. In-depth studies of the cohesin complex and individual subunits could prove instrumental in making progress on the causes of aneuploidy.

1.4 THE COHESIN COMPLEX

1.4.1 Identification of the cohesin complex

The mitotic cohesin complex is made up of four protein subunits, SMC1, SMC3, SCC3 and RAD21 (Figure 1.3), all of which have identifiable homologues in all other eukaryotes studied to date (Nasmyth *et al*., 2001) (Table 1.1). Cohesin components were first identified in budding yeast; *Mcd1*/*Rad21/Scc1* was identified in genetic screens for genes involved in chromosome structure and later found to be essential for chromosome condensation and cohesion (Jachymczyk *et al*., 1977; Birkenbihl and Subramani., 1995; Guacci *et al*., 1997; Furuya *et al.*, 1998; Uhlmann *et al.*, 1999). The Smc1 subunit was initially identified as a protein necessary for nuclear division (Strunnikov *et al.*, 1993) and later the Smc1, Smc3 and Scc1 subunits were discovered in a genetic screen for high frequency loss of chromosomes in the absence of Anaphase Promoting Complex (APC) function (Michaelis *et al*., 1997). The Scc3 cohesin subunit was first identified by Tóth *et al.* (1998), in a screen for genes that permitted nuclear division in the presence of anaphase inhibitor Pds1/Cut2. The nature of the cohesin complex began to emerge when it was demonstrated that Scc1 requires Smc1 to associate with chromatin (Michaelis *et al*., 1997). This was followed by purification of a multisubunit complex containing Scc1, Smc1, Smc3 and two other proteins from *Xenopus* cell

extracts (Losada *et al.*, 1998). Cells carrying mutations in components of the cohesin complex display high frequency chromosome missegregation. In the presence of a functional SAC, these cells undergo arrest due to an inability to align chromosome pairs at the metaphase plate and/or segregate the chromosomes (Michaelis *et al*. 1997).

Meiotic-specific cohesin isoforms have been identified in vertebrates for the SMC1 (SMC1β), RAD21 (REC8) and SCC3 (STAG3) subunits (Revenkova *et al*., 2004; Xu *et al*., 2004; Watanabe and Nurse, 1999). Cohesin complexes containing these alternative subunits are only found in meiotic cells, whereas 'mitotic' cohesin complexes are observed in both mitotic and meiotic cells. The cohesin complex also has two associated proteins ECO1/CTF7 and PDS5, which are not considered subunits but are essential for the regulation of cohesin dynamics (Skibbens *et al.*, 1999; Panizza *et al.*, 2000).

Table 1.2: Cohesin nomenclature in various model organisms.

	S. cerevisiae	*S. pombe*	*D. melanogaster*	*X. laevis*	*M. musculus*	*H. sapiens*
SMC1α	Smc1	Psm1	SMC1	SMC1	SMC1α	SMC1α
SMC1β	*n.p.*	*n.p.*	*n.p.*	*n.i.*	SMC1β	SMC1β
SMC3	Smc3	Psm3	SMC3	SMC3	SMC3	SMC3
SCC1	Mcd1/Scc1	Rad21	dRAD21	xRAD21	mRAD21	hRAD21
REC8	*n.p.*	Rec8	*n.p.*	REC8	REC8	REC8
SCC3	Scc3	Psc3	SA SA2	STAG1 STAG2	STAG1 STAG2	STAG1 STAG2
STAG3	*n.p.*	Rec11	*n.i.*	STAG3	STAG3	STAG3
ECO1	Eco1	Eso1	DECO *n.i.* SAN	*n.i.* ECO2 *n.i.*	ESCO1 ESCO2 NAT13	ESCO1 ESCO2 NAT13
PDS5	Pds5	Pds5	PDS5 *n.i.*	PDS5A PDS5B	PDS5A PDS5B	PDS5A PDS5B
SCC2	Scc2	Mis4	NIPPEDB	xSCC2	NIPBL	NIPBL
SCC4	Scc4	Ssl3	dMAU-2	SCC4	*n.i.*	hMAU-2

n.i. – Not yet identified in this species
n.p. – Not present in this species

1.4.2 The SMC subunits: SMC1 and SMC3

The structural maintenance of chromosomes (SMC) proteins is a diverse family of proteins with a conserved SMC structure with globular amino- and carboxy-termini joined by long α-helical regions. A hinge domain in the centre allows each protein to fold back on itself to form a long rod-shaped molecule with the globular amino- and carboxy-termini joining to form an ABC-like ATPase domain. The two cohesin SMC proteins, SMC1 and SMC3, interact via their hinge regions to form a V-shaped heterodimer (Figure 1.3) (Anderson *et al*., 2002) and some lines of investigation have suggested that the SMC1 and SMC3 ATPase domains are also able to interact directly and form a closed ring independently of the RAD21 subunit (McIntyre *et al.*, 2007; Weitzer *et al*., 2003). ATP hydrolysis at the SMC ATPase head is stimulated by the carboxy-terminal winged-helix domain of the Scc1 subunit in *S. cerevisiae* (Arumugam *et al*., 2006) and this hydrolysis may facilitate opening of the SMC1/SMC3 heterodimer hinge domain to allow the ring complex to encircle DNA strands (Gruber *et al*., 2006; Aruguman *et al*., 2003l Weitzer *et al*., 2003).

In bacteria, a single SMC homodimer complex has been identified that influences chromosome compaction and segregation and is potentially a key player in super-coiling (Grauman and Knust, 2009). In contrast, three distinct SMC complexes exist in metazoans: the condensin complex (SMC2-SMC4 heterodimer), cohesin complex (SMC1-SMC3 heterodimer), and the SMC5-SMC6 heterodimer. Condensin has demonstrated chromosome condensation and dosage compensation functions (Hirano *et al.*, 1997; Jessberger *et al*., 1998). The cohesin complex (SMC1-SMC3) is involved in chromosome cohesion and homologous recombination (Michaelis *et al*., 1997; Losada *et al*., 1998), while the SMC5-SMC6 complex has been linked to DNA damage repair, sister-chromatid recombination (Michaelis *et al*., 1997; Jessberger *et al*., 1998; Losada *et al*., 1998; Torres-Rosell *et al*. 2005; Piccoli *et al.*, 2009) and appears to form an integral Separase-independent cohesin removal mechanism (Outwin *et al*., 2009).

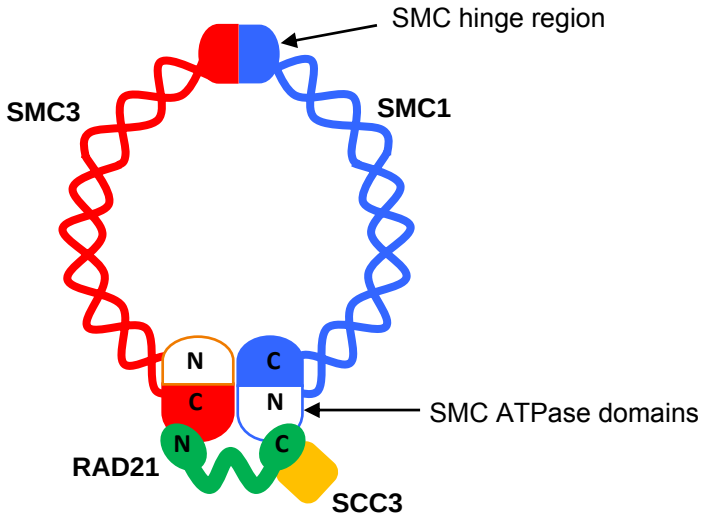

Figure 1.3: The mitotic cohesin complex. Cohesin complexes consist of four proteins. The two structural maintenance of chromosomes (SMC) subunits, SMC1 and SMC3, form a heterodimer via their hinge regions and ATPase domains. The SCC1/RAD21 subunit binds to the globular terminal domains of SMC1-SMC3 and also interacts with the fourth subunit, SCC3.

1.4.3 Kleisins

The subunit referred to as RAD21/Scc1 belongs to a family of proteins referred to as α-kleisins (Schleiffer *et al*., 2003; Haering and Nasmyth, 2003) that binds to the globular ATPase heads of the SMCs via its conserved amino- and carboxy-terminal regions. The RAD21/Scc1 amino terminus binds to the SMC3 subunit, while the carboxy-terminus binds the SMC1 subunit in the cohesin ring (Figure 1.3). The conservation of amino acid sequences at only the amino- and carboxy-terminal domains in all identified kleisins (α and γ families) (Figure 1.4A) and exclusive association with SMC proteins indicates that all SMC dimer pairs are likely to have an associated kleisin subunit and form ring structures (Figure 1.4B) (Schleiffer *et al*., 2003). In yeast the cohesin ring is removed from chromosomes by proteolytic cleavage of the kleisin subunit (Rad21 or Rec8) by the cysteine protease Separase. Only members of the kleisin-α family are known to be proteolytically cleaved in this way (Kudo *et al*., 2006; Buonomo *et al*., 2000; Yanagida, 2000; Uhlmann, 2001; Uhlmann *et al*., 1999).

The RAD21/Scc1 kleisin subunit was first identified in yeast as a mitotic cohesin complex factor, however, in both yeast and mammals it has also been demonstrated to bind to meiotic chromosomes (Xu *et al*., 2004). REC8 is a meiosis-specific kleisin with significant amino acid sequence similarity to RAD21 and is essential for the reductional chromosome segregation of meiosis (Watanabe and Nurse, 1999). RAD21 has been demonstrated to be necessary for the bipolar positioning of sister-chromatids at the metaphase plate, where sister kinetochores are attached to opposite spindle poles. In contrast, REC8 has been demonstrated to be responsible for monopolar positioning of sister-chromatids in MI, where the sister kinetochores are attached to the same spindle pole (Figure 1.4C) (Watanabe and Nurse, 1999; Yokobayashi *et al*., 2003). These spindle orientations are crucial for the correct segregation of the chromosomes.

The requirement for both RAD21- and REC8-containg cohesin complexes in meiotic mammalian cells can be explained in part by their differential chromosomal binding sites adjacent to the kinetochores (Allshire, 1997; Watanabe and Nurse, 1999; Eijpe *et al*., 2003; Kitajima *et al*., 2003; Xu *et al*., 2004). Both REC8 and RAD21 are found at the centromere during MI and MII, where each has unique binding sites and distinct roles in cohesion and kinetochore orientation. These discrete sites of localisation indicate that the subunit composition of the cohesin complex is important for regulation, however, current knowledge cannot sufficiently explain how this regulation occurs. REC8 has been demonstrated to have key roles in homologue pairing, synaptonemal complex (SC) formation and meiotic recombination (Brar *et al*., 2009), thereby covering many of the additional logistical requirements that are present in meiosis but not mitosis.

1.4.4 The Scc3 subunit

SCC3, the fourth cohesin subunit, is also highly conserved among multicellular eukaryotes and is part of the stromal antigen (SA) family of proteins. Three isoforms (SA1, SA2 and STAG3) have been identified in vertebrates, two isoforms in *Drosophila* and only one isoform in both budding and fission yeast (Losada *et al*., 2000; Prieto *et al*., 2001). STAG3 is a meiosis-specific isoform, whereas SA1 and SA2 are both found specifically in mitotic cohesin complexes (Pezzi *et al.,* 2000).

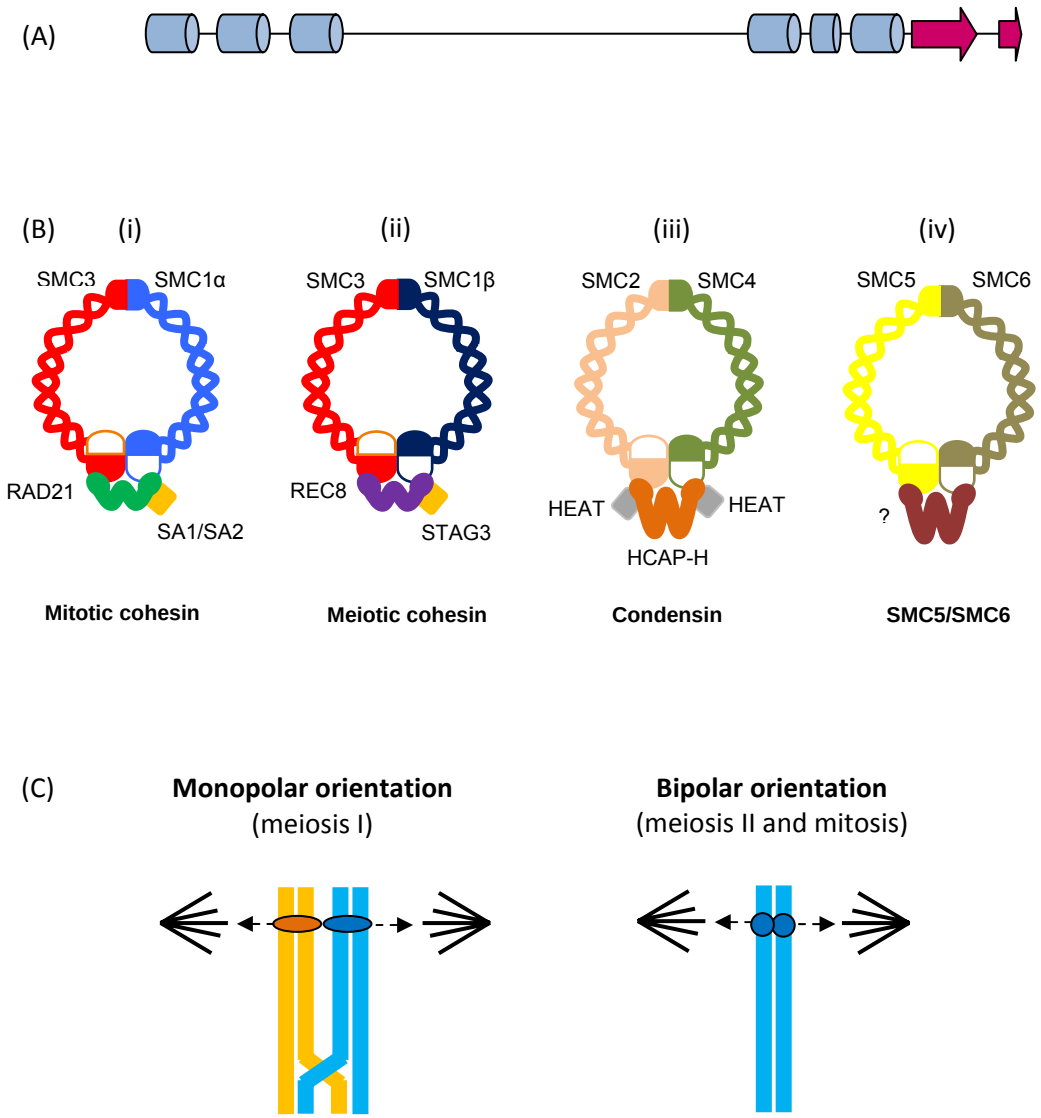

Figure 1.4: Human SMC complexes. (A) The conserved SMC-binding amino- and carboxy-terminal domains of the kleisin protein superfamily (α-helices in blue and β-sheets in red), the central unconserved region is of variable sequence and length between species and family members. (B) Human mitotic cohesin complex with RAD21 α-kleisin (i); human meiotic cohesin with REC8 α-kleisin (ii); human SMC2/SMC4 complex with HCAP-H γ-kleisin (iii); human SMC5/SMC6 complex with a predicted kleisin, currently unidentified (iv). (C) Monopolar orientation of homologous chromosomes in meiosis I directs sister-chromatids to the same spindle pole (i), in contrast in meiosis II and mitosis the sister-chromatids become bipolar oriented and segregate to opposite spindle poles (ii).

The ratio of SA1 and SA2 containing cohesin complexes varies throughout *Xenopus* development, with SA1 being the predominant form in embryos (Losada *et al*., 2000). SA1 and SA2 also display differential nuclear localisation patterns, with SA1 localising directly to chromatin, while SA2 appears to localise to the nuclear envelope (Losada *et al*., 2000). The SCC3/SA subunit binds to the carboxy-terminal region of RAD21/SCC1 in the yeast cohesin complexes (Figure 1.3). While the exact role of the SCC3/SA subunit remains to be fully defined, the variations in isoforms and temporal and spatial expression pattern variation indicate a likely role for SCC3/SA as a regulatory subunit.

1.4.5 Cohesin forms a ring structure

Although many models have been presented to explain how cohesin modulates sister chromatid cohesion, the majority of evidence indicates that the cohesin complex forms a ring-like quaternary structure (Figure 1.5) (Gruber *et al*., 2003; Ivanov and Nasmyth, 2005; Ivanov and Nasmyth, 2007; Haering *et al*., 2008). Cohesin is believed to either enclose both sister-chromatids following replication of the chromosomes or to concatenate sister-chromatids through the linking of multiple cohesin rings. Current evidence indicates cohesin molecules form locked rings that are sufficiently sizeable to encompass two sister chromatids (Figure 1.5B(i)), providing the simplest explanation for how cleavage of the RAD21 subunit could result in release of the sister-chromatid cohesion (Figure 1.5A) (Haering *et al*., 2008). An alternative "handcuff" model has been proposed (Figure 1.5B(ii)) (Zhang *et al*., 2008), where individual cohesin rings circle single DNA helices. This model is hypothesised to provide the flexibility cohesin requires to accommodate other cellular functions such as DNA repair and transcription that occur while cohesin is bound to chromosomes; a flexibility that is thought to be lacking in the single ring model. The cellular reality may be that different conformations of cohesin rings are necessary to achieve the varied roles that cohesin fulfills in chromosome cohesion, DNA repair and transcription regulation.

Although the finer details of how cohesin acts at the molecular level are still unresolved, cohesin has been conclusively demonstrated to be capable of linking DNA molecules and is required to establish and maintain sister-chromatid cohesion. The cellular cohesin population is highly dynamic and is regulated by many different

factors. Cleavage of the RAD21 subunit allows the cohesin ring to open and dissociate from the chromatids, thereby allowing them to separate to separate and segregate to their respective spindle poles (Figure 1.5A). This hypothesised mechanism is supported by experiments where the ring was artificially "opened" by cleaving the SMC3 subunits using a tobacco etch virus (TEV) protease and TEV cleavage sites inserted into the coiled-coil of the SMC3 protein (Gruber *et al*., 2003; Ivanov and Nasmyth, 2005). Exactly how this opening is achieved is unclear as it has long been assumed that the cleavage provides an opening at the ATPase heads. However, it has also been hypothesised that the RAD21 subunit may actually regulate the opening of the hinge region and that removal of the amino-terminal portion of RAD21 alters hinge dynamics (Shintomi and Hirano, 2007).

1.4.6 Identified binding sites

In the search for cohesin binding sites, initial indicators pointed towards there being no cohesin-specific DNA sequence motif. In yeast cohesin complexes seemed to be mainly found at A-T rich regions located on average every 10-15kb apart. Closer analysis of the binding sites revealed that cohesin largely associates with chromosomes at intergenic regions, which in *S. cerevisiae* happen to be A-T rich (Tanaka *et al*. 1999; Laloraya *et al*. 2000). This is believed to support the concept that cohesin binding and active transcription must be mutually exclusive, as the cohesion ring is too small to physically accommodate the transcription machinery passing through it. However, as *de novo* cohesin binding has not been demonstrated to occur between S phase and anaphase, cohesin complexes may simply migrate to transcriptionally silent loci and intergenic regions to accommodate active transcription. Evidence from yeast studies provides support for this notion, with cohesin complexes being translocated from their original loading sites to mainly congregate in the non-coding regions at the ends of converging transcriptionally active genes (Bausch *et al*., 2007; Lengronne *et al*. 2004); presumably having been pushed there by the transcription machinery. In contrast to yeast, studies in *Drosophila* and human cells have found that the loading factor NippedB (NIBL) and cohesin colocalise on chromosomes at transcriptionally active sites (Misulovin *et al*., 2008; Dorsett *et al.,* 2005). Recruitment of cohesin to these sites appears to be dependent on the SCC3/SA subunit interacting with the CCTC- binding factor,

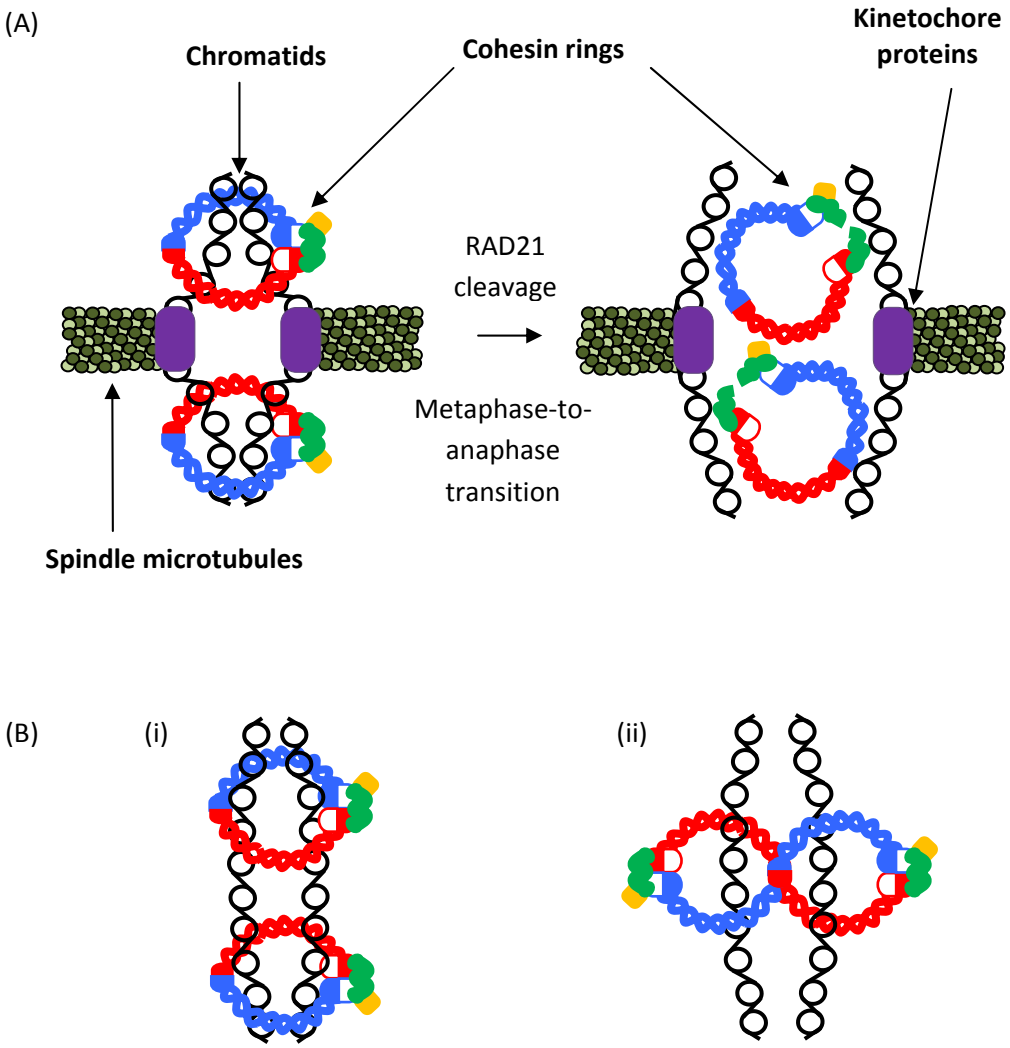

Figure 1.5: Cohesin and the sister chromatid cohesion model. (A) The cohesin rings encircle the sister chromatids (black) following replication of the genome. This cohesive force is sufficient to oppose the pulling forces of the spindle microtubules (light and dark green) attached to the kinetochore of each chromatid. At the onset of anaphase Separase cleaves the RAD21 subunit of the cohesin rings and the sister chromatids are released. (B) Proposed models for cohesin engagement of chromatids: (i) the widely accepted model where a single ring encompasses both chromatids and (ii) the "hand-cuff" model where single rings encompass single chromatids, with interaction between cohesin subunits/motifs to achieve cohesion. (Adapted from Nasmyth and Schleiffer, 2004).

CTCF (Rubio *et al*., 2008; Parelho *et al*., 2008; Wendt et al., 2008). CTCF has demonstrated insulator functions, a role in which NippedB and cohesin have now been implicated (Rubio *et al*., 2008; Gause *et al.*, 2008). Although there is a strong association between cohesin localisation and CTCF, cohesin does not exclusively colocalise with CTCF. It is also currently unclear as to whether CTCF is associated only with cohesin to facilitate transcription regulation or whether there are additional roles in chromosome cohesion.

A study performed in human cells found that cohesin complexes appeared to be recruited to Alu repeats by the chromatin remodelling factor SNF2h (Hakimi *et al*. 2002). Alu repeats fall into the class of short interspersed DNA elements, with approximately 500,000 copies per cell of the 300-bp dimeric sequence comprising ~10% of human genomic DNA (Shankar *et al*., 2009). Interestingly, Alu elements are G-C rich, which is in complete contrast to the A-T rich cohesin binding regions identified in yeast (Hakimi *et al*. 2002). Multiple cohesin loading factors and site variation may explain the differences observed at identified cohesin binding sites. The Alu repeats appear to be associated with specific loci and may correlate with the general transcription activity of the gene. SNF2h and RAD21 are found to both locate to Alu elements and RAD21 binding is dependent on SNF2h and its ATPase activity (Hakimi *et al*. 2002). Histone methylation and acetylation levels appear to be important factors in SNF2h and Rad21 binding, with experiments using the DNA methyltransferase inhibitor 5-azacytidine to decrease methylation resulting in recruitment of RAD21 to Alu sites where SNF2h alone had been localised before (Hakimi *et al*. 2002). Similar to the specific methylation observed at centromeres, methylation of histone H3 lysine four (K4) correlates with SNF2h binding to chromatin. Additionally, acetylation of H3 and/or H4 underlines the importance of histone modification in cohesin loading. The absolute necessity for SNF2h ATPase activity in cohesin binding suggests that chromatin remodeling is an essential step in cohesin association (Hakimi *et al*. 2002). Further support for the chromatin-structure hypothesis is the finding that cohesin shows greatly increased general affinity to chromatin over naked DNA and that recognised cohesin binding sites in yeast do not have a conserved sequence, but instead show conservation of nucleosome structure (Kagansky *et al*., 2004).

1.4.7 Cohesin loading

Cohesin complexes are not capable of spontaneously associating with chromatin. Instead, cohesin requires other factors to facilitate loading onto chromatin in a cell cycle-specific manner, and Scc1 and Scc3/SA are not capable of binding to chromatin in the absence of the SMC subunits. SMC1 and SMC3 bind to DNA via their C-terminal domains, however, chromatin localisation is notably increased when all fours subunits of the cohesin complex are present (Akhmedov *et al*., 1998; Toth *et al,*. 1999; Ciosk *et al*. 2000). Exactly how the cohesin ring functions to open, encompass the DNA strands, and then close and maintain cohesion has been the subject of several investigations. Several studies have shed light on this mystery by demonstrating that the ATPase heads of SMC1 and SMC3 interact directly and functionally bind ATP (Arumugam *et al*., 2003; Weitzer *et al*., 2003). ATP hydrolysis is believed to facilitate both opening and closing of the cohesin ring to allow binding to DNA (Arumugam *et al*., 2003; Weitzer *et al*., 2003), although whether this opening occurs at the ATPase heads or at the hinge regions remains to be determined conclusively (Milutinovich *et al*., 2007; Gruber *et al*., 2006; Hirano and Hirano, 2006).

The proteins Scc2 and Scc4 form a complex that has been identified as a cohesin loading factor in budding yeast that is present throughout the cell cycle (Ciosk *et al*., 2000). Homologues of Scc2 and Scc4 have been identified in fission yeast and some metazoans (Seitan *et al*., 2006; Watrin *et al*., 2006; Bernard *et al*., 2006; Krantz *et al*., 2004; Dorsett, 2004). Scc2 is a member of the Adherin family of proteins, which have now been suggested to promote the ATP-hydrolysis activity of SMC1/SMC3 and thus facilitate cohesion ring opening and chromatin loading (Arumugam *et al*., 2003; Weitzer *et al*. 2003). Scc2 promotion of cohesin ATPase activity and opening of the cohesin ring suggests a direct interaction. Surprisingly, Scc2 and cohesin components have not been shown to co-immunoprecipitate, and therefore any direct interaction is likely to be transient. Also, yeast Scc2 and cohesin fail to co-localise on chromatin (Ciosk *et al*., 2000) making it difficult to accurately hypothesise a loading mechanism for cohesin.

As cohesin has been found to preferentially bind at sites of convergent transcription in genome wide mapping experiments, it is possible that the Scc2/Scc4 interaction

with cohesin is very transient with subsequent translocation of cohesin complexes by the transcription machinery (Glynn *et al*., 2004; Lengronne *et al*., 2004). Studies of the *Drosophila* Scc2 homologue, NippedB, have also failed to demonstrate co-immunoprecipitation with cohesin. However, it has been clearly shown that cohesin and NippedB colocalise on chromosomes, preferentially at sites of active transcription (Misulovin *et al*., 2008). It may be that the more open conformation of actively transcribed DNA is amenable cohesin loading; however, cohesin and NippedB have also been linked functionally in regulation of transcription. Together cohesin and NippedB regulate gene expression by as yet unconfirmed mechanisms, with current evidence indicating a role in modification of long range enhancer element interactions with target genes (Wendt *et al*., 2008). This may reflect a cooperative role in regulation of gene expression which is not present in yeast. Consistent with this, mutations in the human homologue of Scc2, NIPBL, have been linked to Cornelia de Lange syndrome, a rare multisystem developmental disorder that also shows variable somatic karyotype abnormalities (Krantz, *et al*., 2004; Tonkin *et al*., 2004).

Scc2 and Scc4 are both essential for the loading of yeast cohesin on both chromosome arms and at centromeres, suggestive of a conserved functional role in these distinct chromatin domains (Ciosk *et al*., 2000). Other lines of evidence indicate that the metazoan Scc2/NippedB homologues are not always required for cohesin loading, in particular at centromeric sites. Scc2-independent loading of yeast cohesin has been observed when a population of cohesin appears to be dislodged from the chromatin by the transcription machinery and is then reloaded, but no longer confers cohesion between sister-chromatids (Bausch *et al.*, 2007). Scc2-independent loading also occurs when the centromeric region of pre-anaphase chromosomes undergoes "breathing", where the chromatids transiently separate a greater distance than can be encompassed by cohesin rings (Ocampo-Hafalla *et al.*, 2007). The centromeric region appears to provide a unique cohesin binding environment in metazoans that is differentially regulated compared to chromosomes arms. In *Drosophila* at least, NippedB does not appear to be essential for loading of cohesin at the centromeres of meiotic chromosomes (Gause *et al*., 2008). Additionally, other factors involved in heterochromatin and kinetochore formation, such as histone H3 variant CENP-A (Cse4/Cid) and heterochromatin protein HP1

(Swi6), are associated with the concentrated centromeric loading of cohesin (Eckert *et al.*, 2007; Bernard *et al*., 2001). Swi6 has been found to co-immunoprecipitate with Mis4, the fission yeast Scc2 homologue (Fischer *et al*., 2009), confirming a direct link between Swi6 activity and cohesin loading.

1.4.8 Establishment of cohesion

The binding of cohesin to chromatin is necessary but not sufficient for the establishment of cohesion between chromatids. Instead a number of factors, including Eco1/Ctf7, Wpl1 and Pds5, are also required to "lock" the cohesin ring around the sister-chromatids, thereby tethering them together. Although cohesin is observed to associate with chromatin from telophase (in metazoans) or late G1 phase (in yeast), cohesion is only established with the aid of Eco1/Ctf7 once the chromosomes are replicated in S phase (Brand and Skibbens, 2005). After cohesion is established in S phase ECO1 is not required for cohesion maintenance throughout the G2 and M phases (Toth *et al*. 1999). Mutations in the human ESCO1 gene are linked to Roberts Syndrome, a multisystem developmental disorder with patients displaying chromosomal defects (McDaniel *et al*. 2005; Vega *et al*. 2005; Gordillo *et al.*, 2008). Eco1 encodes an acetyltransferase that has been demonstrated to acetylate the Mcd1 (Rad21) and Smc3 subunits of yeast cohesin to antagonise the cohesin displacing activities of Wpl1 (Wapl) (Heidinger-Pauli *et al.*, 2009; Ivanov *et al*., 2002). During S phase, when cohesion is established, the Smc3 cohesin subunit is acetylated by Eco1, causing the Wpl1-Pds5 regulatory complex to temporarily dissociate from cohesin complexes and thereby allowing cohesin rings to functionally engage with sister-chromatids (Rowland *et al.*, 2009; Sutani *et al*., 2009). Wpl1 normally inhibits cohesion establishment post S phase, however, Eco1 is able to antagonise Wpl1p activity in response to DNA double-stranded breaks during G2/M through acetylation of Mcd1, resulting in genome-wide loading of cohesive cohesin (Heidinger-Pauli *et al.*, 2009).

Loading of cohesin and establishment of cohesion have been closely linked to DNA replication, with further support coming from studies showing that DNA polymerases are also needed for effective sister-chromatid cohesion (Uhlmann and Nasmyth, 1998). *S. cerervisiae* polymerase ε (Pol 2) has an amino-terminal region

with essential DNA polymerase activity, while the C-terminal region interacts with polymerase σ, which acts to significantly increase the polymerase activity of the polymerase ε holoenzyme. Two redundant genes, Trf4 and Trf5, which are also nucleotidyl transferases, encode polymerase σ. Trf4 has demonstrated functions in sister-chromatid cohesion, completion of S phase and DNA repair, and potentially functions in cohesin loading by competing with the RNA helicase Dbp2 for binding to Pol 2, where it may affect transient remodelling at the replication fork and thereby allow interaction with cohesins (Wang *et al*. 2000). Pol 2 has also been shown to interact with Smc1 and Eco1/Ctf7, providing a link between progression of the replication fork and establishment of cohesion (Edwards *et al*. 2003).

Although the exact mechanisms are still being elucidated, there is a clear link between activity at the replication fork and cohesin loading and establishment. In *S. cerevisiae*, Ctf18 and Elg1 form alternative replication factor C (RFC) and RFC-like (RLC) protein complexes, respectively, in conjunction with the small RFC subunits Rfc2-5 (Parnas *et al*., 2009; Bellaoui *et al*., 2003). These complexes are present at the replication fork with Eco1, being required for sister-chromatid cohesion and DNA repair (Maradeo and Skibbens, 2009; Bellaoui *et al*., 2003; Mayer *et al*. 2001). The RFC and RLC complexes act as clamp loaders for DNA replication clamps, including PCNA (pol30), and may be involved with polymerase switching at sites of cohesin binding (Mayer *et al*. 2001). PCNA is a DNA polymerase processivity factor that stabilises polymerase association with DNA, and over-expression of PCNA is found to partially rescue the effects arising from loss of Eco1/Ctf7 (Skibbens *et al*. 1999). Ctf7 physically interacts with both PCNA and the RFC/RLC complexes (Moldovan *et al*., 2006; Majika and Burgers, 2004; Skibbens, 2005; Kenna and Skibbens, 2003), however, these appear to represent redundant cohesin loading mechanisms as mutations in PCNA and RFC/RLC components produce approximately 1/2-1/3 of the cohesion defects observed in cohesin subunit mutants or Eco1/Ctf7 mutants (Guacci *et al*., 1997; Michaelis *et al*., 1997; Skibbens *et al*., 1999; Toth *et al*., 1999; Moldovan *et al*., 2006; Mayer *et al*., 2001; Kenna and Skibbens, 2003; Edwards *et al*., 2003). Another protein, Ctf4, is present with the RFC and/or RLC and Eco1 at the replication fork during S phase and is thought to be a central figure in coordinating DNA replication, checkpoint activation,

chromosome cohesion and DNA damage repair (Yoshizawa-Sugata and Masai, 2009). The current hypothesised models involve Eco1-driven partial dismantling of the replication fork to allow passage through a single cohesin ring. Alternatively, single cohesin rings may be transiently opened in an Eco1-Pds5-dependent manner, or potentially Eco1 and Pds5 regulate pre-loaded cohesin ring opening/closing while driving ring-ring interactions with newly loaded cohesin rings in a catenation cohesion model (Skibbens *et al*., 2007).

1.4.9 Cohesin dynamics and cohesion maintenance

Following DNA replication, cohesion is maintained via the interplay of three cohesin maintenance factors: Wapl (Wpl1), Sororin and Pds5. These proteins are considered regulatory subunits of the cohesin complex as they coimmunoprecipitate with cohesin complexes from HeLa cells and are dependent on cohesin for their association with chromatin (Losada *et al*., 2005; Sumara *et al.*, 2000; Rankin *et al*., 2005; Kueng *et al.*, 2006; Gandhi *et al*., 2006). In yeast cells Wpl1 and Pds5 have been found to form a regulatory heterodimer that acts an "anti-establishment" factor for cohesin mediated cohesion (Sutani *et al*., 2009). Ctf7 and Pds5 have also been found to coimmunoprecipitate from yeast cells, with overexpression of either protein able to suppress the temperature sensitivity of the reciprocal mutant (Noble *et al.*, 2006). These interactions suggest that Pds5 has a role in cohesion establishment as well as cohesion maintenance. This role was first recognised for Pds5 in budding yeast, where loss of Pds5 results in premature chromatid separation and abnormal chromosome condensation (Hartman *et al*., 2000; Stead *et al*., 2003), and has more recently been shown to result in failure of homologue synapsis during meiosis (Jin *et al.,* 2009). Pds5 clearly has a complex regulatory role in metazoan cohesin dynamics, for although Pds5 colocalises with cohesin throughout the cell cycle the reduction of Pds5 has varying effects on chromosome segregation. In human HeLa cells reduction of Pds5 results in premature chromosome separation, while mitotic chromosomes in *Xenopus* egg extracts lacking Pds5 do not suffer loss of cohesion at the chromosomes arms, show only a loosening of cohesin at centromeres, and retain a high level of cohesin on chromosomes into mitosis (Losada *et al.*, 2005). Fission yeast Pds5 mutants display hypersensitivity to DNA damage and metaphase delay, as well as some cohesion defects (Wang *et al*., 2002). Mutations in the human Pds5 homolog, PDS5B, cause development disorders and multisystem defects and are

seen in a subset of cases of Cornelia de Lange syndrome that are not associated with mutations in NIPB-L (Dorsett, 2007; Dorsett, 2004). Differences observed in Pds5 function in different species may reflect the nature of mutant alleles examined or reflect species-specific variations in cohesin regulation.

At least two populations of cohesin exist in the cell, stably-bound cohesin, which is predicted to be required for maintaining cohesion, and dynamic cohesin, which cycles rapidly on and off chromatin with uncertain functional consequences. Wapl and Sororin have counteractive effects on the residency time of dynamically- and stably-associated cohesin on chromatin, respectively. Wapl destabilises chromatin binding by the dynamic cohesin population, thereby reducing residency time, preventing cohesion establishment in G1 and promoting cohesin removal from chromatid arms during prophase. Experiments uncoupling the events of cohesin stabilisation and DNA replication may indicate that cohesin stabilisation is required for cohesion establishment rather than the other way round (Bernard *et al*., 2008). The destabilising activities of Wapl are counteracted in S phase by the acetyltransferase activity of Eco1, thereby allowing stabilisation of cohesin association with chromatin and establishment of cohesion (Bernard *et al*., 2008; Ben-Shahar *et al*., 2008; Sutani *et al*., 2009; Rowland *et al*., 2009). Overexpression of Wapl in human cells results in premature sister chromatid separation and chromosome instability, and upregulation of Wapl has been identified in cells infected by human papillomavirus (HPV), which are highly susceptible to tumour progression (Ohbayashi *et al.*, 2007).

Sororin is necessary for maintaining the population of stably bound cohesin and unlike Wapl, has as yet only been identified in metazoans (Díaz-Martínez *et al.*, 2007; Rankin *et al.*, 2005). Sororin is required for the maintenance of chromosome cohesion and DNA damage repair during G2 phase, with Sororin over-expression resulting in failure of sister-chromatids to resolve and segregate at anaphase. Sororin-depleted HeLa cells display complete loss of chromatid cohesion in metaphase and temporary arrest by the spindle checkpoint (Schmitz *et al.*, 2007; Díaz-Martínez *et al.*, 2007; Rankin *et al.*, 2005).

1.4.10 Cohesin dissociation – prophase

In yeast the entire population of chromosome-bound cohesin is cleaved by Separase at the onset of anaphase to facilitate opening of the cohesin ring and separation of the sister-chromatids (Uhlmann *et al.*, 1999; Ciosk *et al.*, 1998). In contrast, in metazoans a prophase dissociation pathway also exists that allows removal of cohesin molecules from the chromosome arms by a non-proteolytic, phosphorylation-dependent mechanism (Figure 1.6). At the onset of anaphase, the small pool of centromeric cohesin and any remaining arm cohesin is removed by separase (Nasmyth and Schleiffer, 2004; Hauf *et al*., 2001; Uhlmann et al., 1999; Ciosk *et al*., 1998). While arm- and centromere-specific mitotic cohesin complexes do not differ in their subunit composition, there are clear differences in the regulation of dissociation of these two populations from chromosomes. The cohesin prophase dissociation pathway involves POLO (PLK1) kinase phosphorylation of the Scc3/SA subunit in combination with the cohesin-destabilising activities of Wapl (Hauf *et al*., 2005; Sumara *et al.*, 2002). Meanwhile, the centromeric cohesin is protected and retained until anaphase when the Scc1/RAD21 subunit is cleaved by Separase. This differential regulation appears to be achieved through protection of centromeric cohesin from phosphorylation by Shugoshin (SGO1/MEIS332) proteins and protein phosphatase 2A (PP2A) activity (Kitajima *et al*., 2006; Riedel *et al*., 2006).

MI comprises a particularly complex situation where there are two differentially regulated segregation events where sister-chromatids are kept together during MI, while allowing homologous chromosomes pairs to separate (Rabitsch *et al*. 2004; McGuinness *et al*. 2005). Current evidence indicates that the Shugoshin proteins and PP2A are responsible for protecting the centromeric cohesins of sister-chromatids from phosphorylation and cleavage during both mitosis and MI (Kitajima *et al*., 2006; Riedel *et al*., 2006; McGuinness *et al*., 2005). SGO1 localises to centromeres at prophase and then disappears at the onset of anaphase as would be expected of a metazoan cohesin-protection protein. Loss of SGO1 function results in loss of cohesin at the centromere and consequently loss of sister-chromatid cohesion causing cells to arrest in a prometaphase-like state. (McGuinness *et al*., 2005). SGO1 localisation at the centromere it determined by the spindle checkpoint protein BUB1, and PP2A and AURORA B kinases.

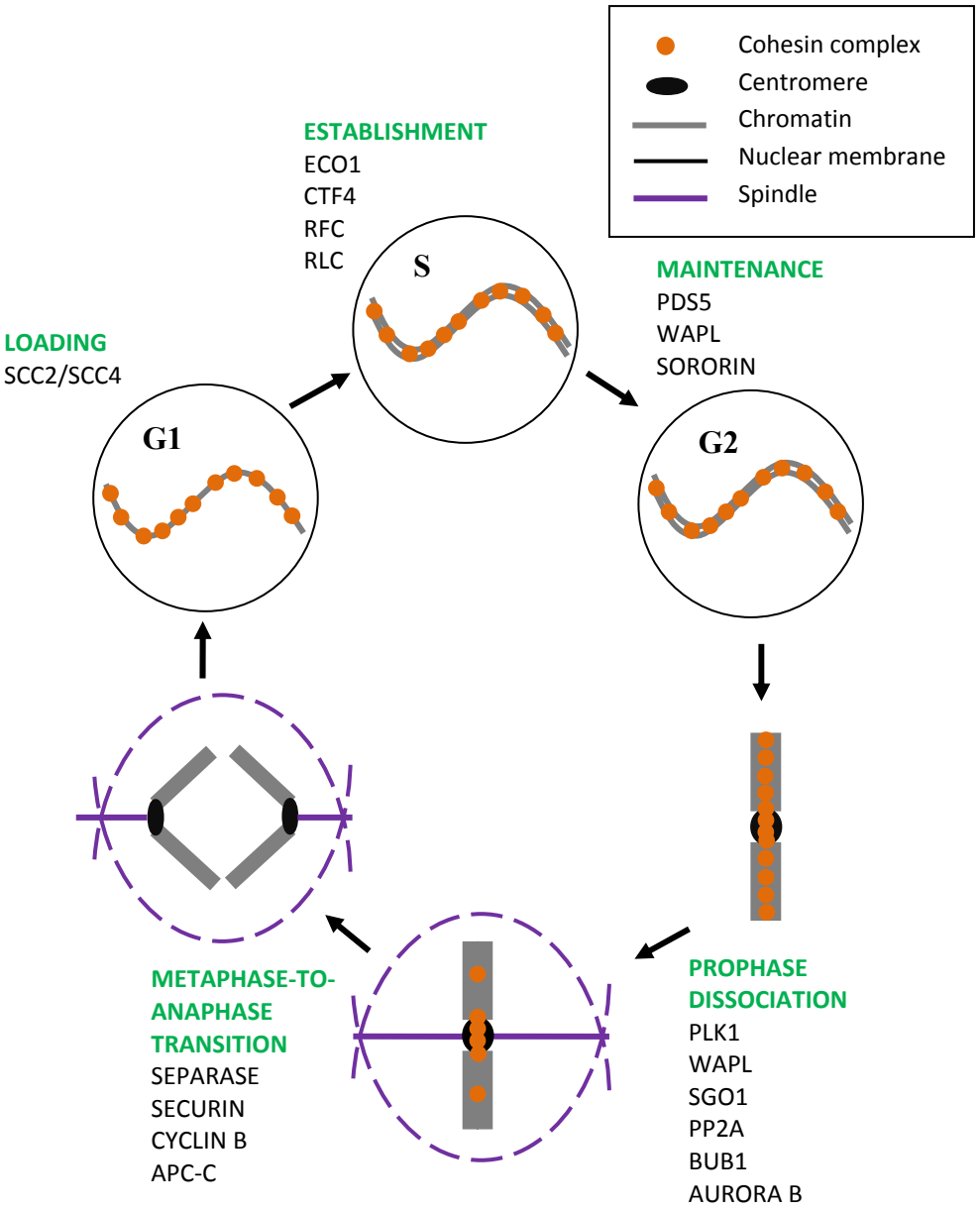

Figure 1.6: Cohesin cell cycle dynamics. Cohesin complexes are regulated through each phase of the cell cycle by a wide variety of proteins. Such tight regulation in loading, maintenance and removal is essential for accurate chromosome segregation.

Additionally, BUB1 and AURORA B centromeric localisation is inter-dependent (Tang *et al.*, 2006; Kawashima *et al.*, 2007; Kitajima *et al.*, 2005; Resnick e*t al.*, 2006) . Loss of BUB1 function results in SGO1 mis-localisation along the entire length of the chromosome (Bernard *et al*., 1998; Basu *et al*., 1999; Kitajima *et al*., 2005). It is quite feasible that protein components of the centromere determine the localisation of BUB1 and AURORA B, which in turn restricts the localisation of SGO1 to the centromere and thereby effects the differential regulation of centromeric cohesin that is observed.

Several other factors have been linked with the cohesin prophase dissociation step; however, less data are currently available for these proteins. Depletion of Hapsin, a histone H3 kinase, or Prohibitin 2 (PHB2) results in premature sister chromatid separation in mitosis. Additionally, overexpression of Haspin rescues the cohesion defect observed in SGO1 depleted cells, while co-depletion of PHB2 and POLO is able to rescue the cohesion defects of PHB2 mutants (Dai *et al*., 2006; Takata *et al*., 2007).

1.4.11 Cohesin dissociation - anaphase

Although the majority of chromatin bound cohesin is removed from metazoan chromatid arms during prophase and prometaphase (Figure 1.6), a fraction of cohesive cohesin remaining on the arms and a significant centromeric pool requires the activity of Separase for complete removal at anaphase (Figure 1.6) (Nakajima *et al.*, 2007; Uhlmann *et al.*, 1999; Ciosk *et al.*, 1998). The protease responsible for cohesin removal, Separase, is held inactive by the regulatory subunit Securin and by inhibitory phosphorylation of Separase by Cdk1-cyclinB. At the onset of anaphase, the Anaphase Promoting Complex/Cyclosome (APC-C) marks securin and cyclin B for degradation by the proteasome via ubiquitylation (Ulhmann, 2001) Once Separase becomes actived it is free to cleave the RAD21/Scc1 component of cohesin complexes bound to the chromatin. *In vitro* studies have also shown cleavage of cohesin is promoted by POLO phosphorylation of the RAD21 subunit of cohesin (Hornig *et al*., 2004; Alexandru *et al*., 2001). RAD21 cleavage by Separase occurs at either or both of two conserved sites within the protein sequence (Figure 1.7). The core consensus cleavage sequence ((DE)XXR/X) is observed in the RAD21 and REC8 homologues from yeast to humans, with the invariant arginine residue (R)

flanking the peptide bond cleaved by Separase (Figure 1.7B). RAD21/Scc1 cleavage leaves the invariant arginine as the carboxy-terminal residue of the amino-terminal cleavage products, with the amino-terminal residue of the peptide fragment being a destabilising residue that targets the peptide for degradation by the ubiquitin/proteosome-dependent N-end rule pathway (Rao *et al*., 2001). Degradation of the carboxy-terminal cleavage peptide is essential for chromosome stability and persistence of this peptide has been found to be lethal in budding yeast cells (Rao *et al*., 2001). Studies in human and yeast cells have found that both of the Separase cleavage sites in RAD21/Scc1 need to be altered in order to inhibit Separase cleavage and chromosome segregation. This inhibition of chromosome segregation resulted in a substantial increase in anaphase bridges and aneuploidy (Toyoda *et al.*, 2002; Hauf *et al.*, 2001; Tomonaga *et al.*, 2000).

(A)

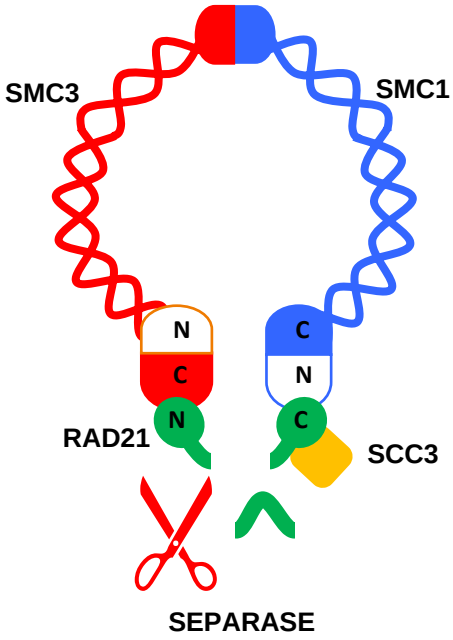

(B)

RAD21	Hs	167	DR**E**IM**R**E	445	IE**E**PS**R**L
	Sc	175	LV**E**VG**R**R	263	SV**E**QG**R**R
	Sp	174	SI**E**AG**R**N	226	SI**E**VG**R**D
	Dm	170	TP**E**II**R**C	469	AP**E**VL**R**A

(C)

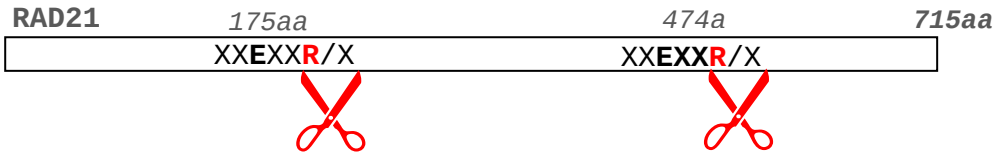

Figure 1.7: Cleavage-dependent cohesin removal. At the metaphase-anaphase transition the APC-C initiates degradation of securin and cyclin B, releasing their inhibition of separase activity. (A) Separase (red scissors) proceeds to cleave the RAD21 subunit of all cohesin complexes remaining on the chromosomes at this time. (B) RAD21 contains two separase cleavage sites, which have a consensus sequence that is evolutionary conserved from yeast to humans (Hs, *Homo sapiens*; Sc, *Saccharomyces cerevisiae*; Sp, *Shizosaccharomyces pombe*; Dm, *Drosophila melanogaster*) in RAD21 and REC8 homologues. (C) Cleavage of the RAD21 Separase sequences occurs immediately after the conserved arginine residue (R).

1.5 *DROSOPHILA MELANOGASTER* AS A MODEL TO STUDY ANEUPLOIDY

1.5.1 Aneuploidy studies in Drosophila

Drosophila melanogaster has a long history of being utilised as a model organism for human aneuploidy research (Birchler *et al*., 2001; Morton *et al.*, 1990; Grell and Valencia, 1964; Dallapiccola *et al.*, 1978). *Drosophila* achiasmate chromosomes mimic the altered recombination and non-disjunction that are believed to underlie some meiotic aneuploidies (Koehler and Hassold, 1998) and have been used extensively to identify genes that influence chromosome inheritance. In-depth studies in *Drosophila* to determine the minimum functional centromere resulted in the development of minichromosomes, a collection of reduced chromosomes with compromised inheritance rates that have also been a key tool in identifying genetic factors that influence chromosome inheritance (Dobie *et al.*, 2001; Sun *et al*., 1997, Cook *et al.*, 1997). More recently a *Drosophila* model system for studying the maternal age effect in older oocytes has been developed (Jeffreys *et al*., 2003). Many genes that normally function to prevent aneuploidy have been discovered and functionally analysed in *Drosophila*, including the kinetochore protein Mitch (Williams *et al.*, 2007), the SAC proteins Rod, Zw-10 , BubR1 and Bub3 (Karess and Glover, 1989; Williams *et al*., 1992; Lopes *et al*., 2005; Logarinho *et al.*, 2004) the checkpoint protein Chk2 (Takada *et al*., 2003), the APC-C subunit ida (Bentley *et al*., 2002), the cell cycle regulator Myb (Manak *et al.*, 2002) and the meiotic recombination protein Ord (Bickel *et al*., 1996).

Induction of aneuploidy has also been studied in *Drosophila* using various chemicals that humans are commonly exposed to or that are informative about cellular mechanisms (Osgood and Cyr, 1998; Ferguson *et al*., 1996; Liang and Brinkley, 1985; Held, 1982; Zimmering, 1982; Traut, 1981; Traut, 1978).

1.5.2 The development of the Drosophila *GMR*>Rad21^{NC} *mutant*

A study was undertaken by Keall (2005), to characterise *Drosophila Rad21* with the view of utilising the *Drosophila* cohesin complex as an instrument for investigating chromosome segregation and aneuploidy. Studies with human and yeast non-cleavable RAD21/Scc1 had demonstrated inhibition of the normal segregation of

chromosomes resulting in a substantial increase in anaphase bridges and aneuploidy (Toyoda *et al.*, 2002; Hauf *et al.*, 2001; Tomonaga *et al.*, 2000). From these data it was hypothesised that ectopic expression of non-cleavable RAD21 ($RAD21^{NC}$) in *Drosophila* should produce similar cellular effects and an observable phenotype. The work of Keall (2005) identified two Separase cleavage sites in the *Drosophila melanogaste*r RAD21 sequence based on their similarity to known RAD21/Scc1 cleavage sites in humans and yeast (Figure 1.7). Mutation of these Separase sites and ectopic expression of the RAD21 cleavage variant transgenes in the developing *Drosophila* eye (Figure 1.8) was indeed observed to result in disturbance of normal tissue development (Keall, 2005).

The Separase cleavage sequence is highly conserved between species, with an invariant arginine residue denoting the point of cleavage, which occurs at the peptide bond between the arginine and the following residue (Figure 1.9). Site-directed mutagenesis of the invariant arginine residues to alanine at the two identified *Drosophila* RAD21 cleavage sites (ie R175 and R474) was the tactic used to inhibit Separase cleavage (Figure 1.9). Ectopic expression in the developing eye of the $RAD21^{N}$ (R175A) protein with the single amino-terminal mutation produced no observable phenotypic effects, in contrast to ectopic expression of the $RAD21^{C}$ (RA474AG) protein with the single carboxy-terminal mutation or $RAD21^{NC}$ (R175A/RA474AG) protein with both sites mutated, which both produced a reduced and disorganised eye phenotype (Figure 1.9). Both the overall size of the eye and the organisation of the ommatidia were severely reduced in the $RAD21^{NC}$ cleavage-mutant transgenics (Keall, 2005). The ability of the $RAD21^{C}$ cleavage variant to produce a mutant phenotype was in contrast to the previous studies in yeast and human cells, as these studies had found mutation of both Separase cleavage sites necessary to produce inhibition of chromosome segregation (Toyoda *et al.*, 2002; Hauf *et al.*, 2001; Tomonaga *et al.*, 2000). The phenotype produced by $RAD21^{C}$ and the lack of phenotype produced by $RAD21^{N}$ led Keall (2005) to speculate that the carboxy-terminal Separase cleavage site was the dominant site of RAD21 cleavage in *Drosophila*.

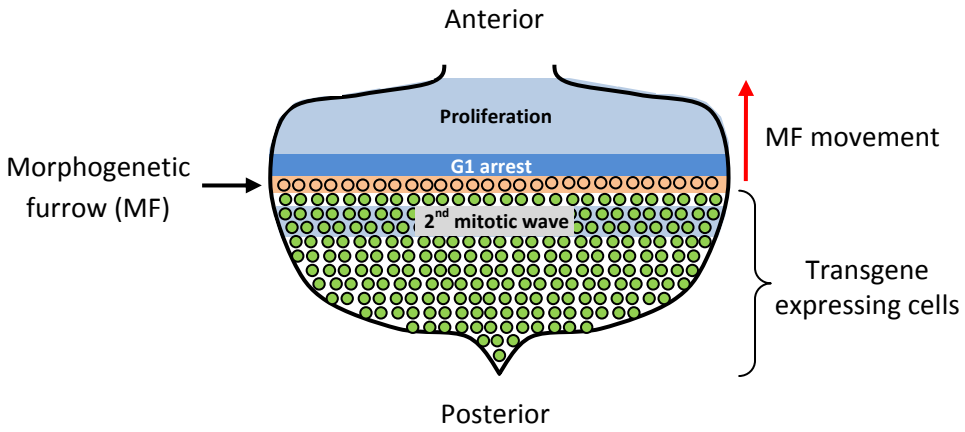

Figure 1.8: *Drosophila* eye development. The compound eye is a particularly useful and powerful organ for performing genetic screens because of its highly organised nature and being unnecessary for viability and fertility. In the developing eye cells proliferate asynchronously until the morphogenetic furrow passes from the posterior to the anterior of the eye-antennal imaginal disc, inducing a G1 arrest ahead that synchronises the cells followed by a final round of division of a subset of cells termed the 2nd mitotic wave. Cells posterior to the MF undergo differentiation as they mature and are recruited to ommatidia. The compound eye contains approximately 750 ommatidia, hexagonal clusters of 11 very specifically arranged cells that are formed into very exact diagonal rows. This array is highly sensitive to perturbations in eye development, such as alterations in cell numbers, ommatidial rotation, and cell recruitment to ommatidia. Transgenes can be ectopically expressed in the eye using a tissue-specific drive and the yeast Gal4-UAS system. The eye-specific driver Glass Multimer Reporter (GMR) uses the eye-specific transcription factor glass (gl) to drive expression of Gal4 in cells posterior to the morphogenetic furrow. Gal4 binds specifically to the Upstream Activated Sequences (UAS) associated with the transgene, thereby allowing expression of the transgene in developing eye cells (green circles). (Adapted from Freeman, 1997).

(A)

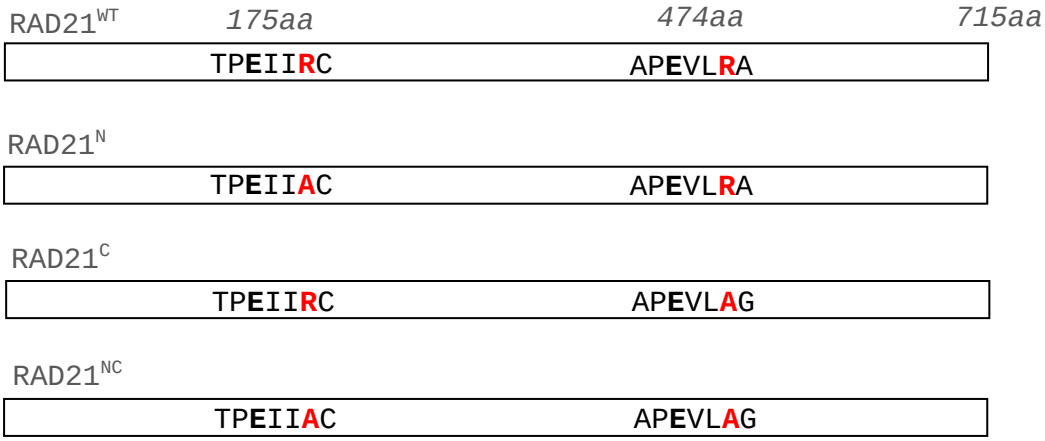

(B)

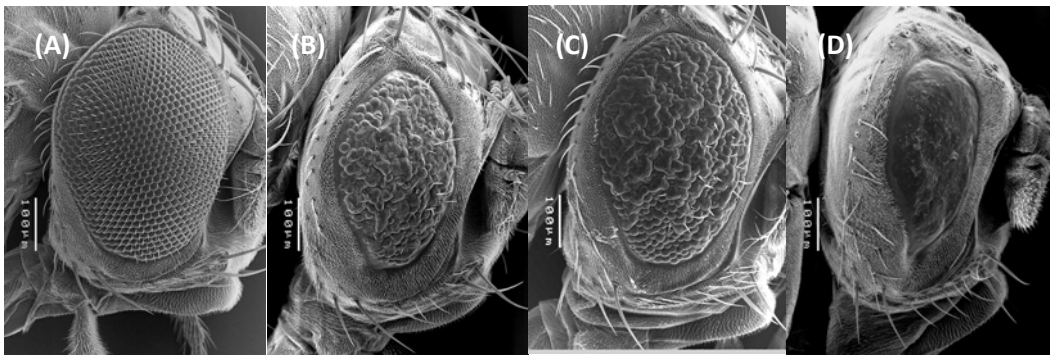

Figure 1.9: ***Drosophila Rad21*** **cleavage variants.** (A) Separase cleavage of the RAD21 protein occurs after the invariant arginine residue (red). The *Drosophila Rad21* cDNA was altered, by site-directed mutagenesis, at one or both of the amino- and carboxy-terminal Separase cleavage sites. At the amino-terminal cleavage site the arginine reside (R) was mutated to alanine (A), while at the carboxy-terminal cleavage site the arginine residue and consecutive alanine (RA) residue were mutated to alanine and glycine (AG). (B) Expression of the double-mutant $Rad21^{NC}$ under the control of the GMR>Gal4 driver resulted in a change in eye phenotype, with significant and reproducible reduction in the size and organisation of the eye (B) compared to a wildtype eye (A). This GMR>$Rad21^{NC}$ mutant eye phenotype was also found to be modifiable in a heterozygous mutant background; with modifiers showing both suppression (GMR>$Rad21^{NC}$/$Egfr^{k05115}$) (C) and enhancement (GMR>$Rad21^{NC}$/dl^{UY2278}) (D).

From the above observations it was hypothesised that cleavage-resistant RAD21 was being incorporated into functional cohesin rings that were inhibiting the segregation of replicated chromosomes. By using markers of mitosis and apoptosis, Keall (2005) showed that there was an increased mitotic index and increased level of apoptosis in the eye-antennal imaginal discs of the *Rad21*^{NC} transgenics, with an eye-specific driver, compared to wildtype. These results are consistent with the cells being unable to segregate their replicated chromosomes and consequently arresting in mitosis and eventually apoptosing due to an inability to resolve the segregating chromatin masses.

One of the strengths of the *Drosophila* system is its utility in performing genome-wide genetic screening. The *Drosophila* GMR>*Rad21*^{NC} model was judged to be a suitable and effective tool to screen for modifiers of chromosome inheritance. This was based on initial observable changes in the GMR>*Rad21*^{NC} rough-eye phenotype when the transgene was expressed in heterozygous mutant backgrounds for genes known to regulate cohesin and chromosome segregation. This preliminary testing of the screening tool was performed by Keall (2005) and included: the RAD21 cleaving protease subunits, *three-rows* and *pimples* (*Separase* homologue); the cohesin loading factor, *NippedB* (*Scc2* homologue); the mitotic cell cycle regulator, *Cyclin B*; and the centromeric cohesin maintenance factors, *polo* kinase and *mei-S332*. These genes were all found to modify the GMR>*Rad21*^{NC} in a manner consistent with and predictable from their known functions.

A genome-wide genetic screen was carried out by Keall (2005), observing whether large chromosomal deletions, when hemizygous, were capable of altering the rough-eye phenotype produced by GMR>*Rad21*^{NC}. In this screen, Keall (2005) used the 'Deficiency Kit' of overlapping deletions to screen more than 90% of the *Drosophila melanogaster* genome. With this approach, 57 interacting regions that either suppressed or enhanced the GMR>*Rad21*^{NC} phenotype (Figure 1.10) were identified. Keall also identified 11 interactors to the gene level in 8 of these regions.

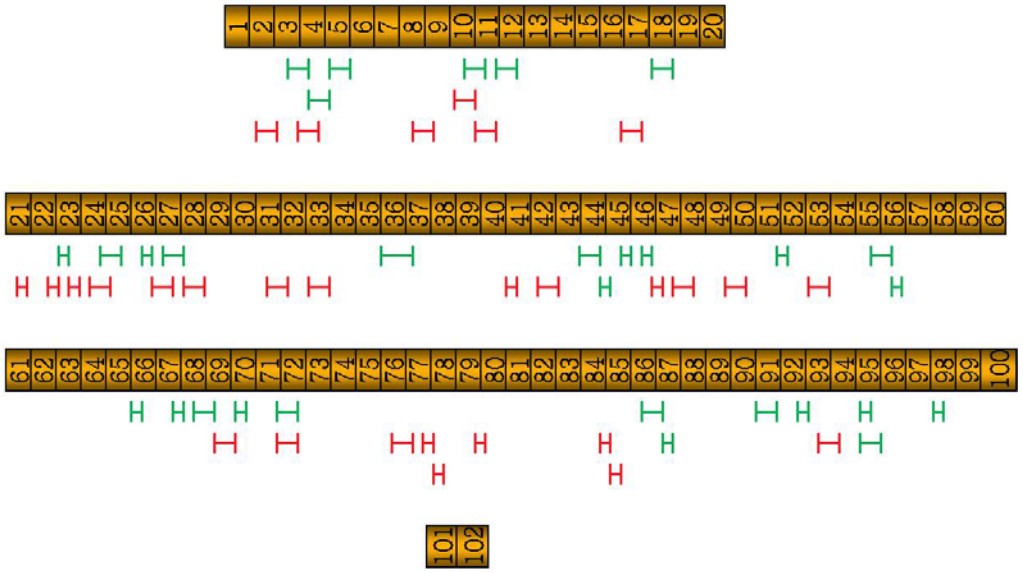

Figure 1.10: Cytological positions of chromosomal deletion regions that modified the GMR>*Rad21*^{NC} rough-eye phenotype. Enhancing deletions are indicated by the red brackets and suppressing deletions are indicated by the green brackets. The size of the bracket is indicative of the size of the deletion.

1.6 THE SCOPE OF THIS PROJECT

All disease manifestations are a combination of an individual's environment, underlying genetics and stochastic events (Figure 1.11). Dissecting the relative contribution of these factors is a complex task that is compounded by the complexity of mammalian genomics and cell biology, and the relative ubiquity of many environmental influences that may contribute to the outcome. Aneuploidy is another instance where many factors influence the outcome. Genetic risk factors have long been recognised for many human diseases; however, knowledge of the molecular mechanisms that contribute to aneuploidy is still relatively scarce. Additionally, despite many decades of research, the vast majority of evidence for the origins of meiotic aneuploidy remains at the macroscopic level of maternal age effect, recombination rates and the incidence of meiotic aneuploidy in human populations. Much additional information is to be garnered regarding the molecular mechanisms behind mitotic and meiotic aneuploidy, and studies in model organisms have and will continue to play a key part of this process.

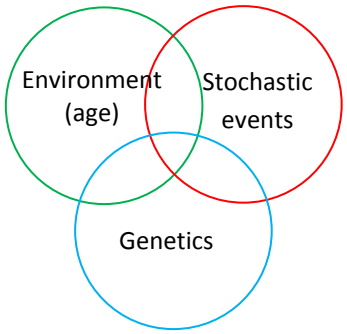

Figure 1.11: Disease manifestation. Disease manifestation is dependent on an individual's age, underlying genetics and their environment.

Following on from the work of Keall (2005) several key issues remained outstanding in the investigation of chromosome cohesion and segregation modifiers using the GMR>*Rad21*^{NC} model. Firstly, it remained to be definitively demonstrated that mutation of the *Drosophila Rad21* Separase cleavage sites resulted in an observable change in RAD21 cleavage patterns and that inhibition of RAD21 cleavage resulted in an observable chromosome segregation phenotype at the cellular level. Secondly, further characterisation of the GMR>*Rad21*^{NC} phenotype was necessary to understand the full extent of the cellular effects of inhibiting chromosome segregation. And finally, the identity of the modifier loci, within the chromosomal regions identified in the original Deficiency Kit screen, remained to be determined at the molecular level.

This project aimed to identify novel modifiers of chromosome segregation and aneuploidy-survival genes using *Drosophila melanogaster* as a model organism. *Drosophila* models offer the benefits of a multicellular system that yeast models lack, without the complexities and costs encountered when working with mammalian models. Homologues for the mitotic cohesin subunits SMC1, SMC3, RAD21 and SA/SCC3 have all been identified in *Drosophila*, along with key cohesin regulators including SCC2, DECO/ECO1, WAPL, POLO and Separase (Williams *et al*., 2003; Verni *et al*., 2000; Warren *et al*., 2000; Jones and Sgouros,

2001; Sunkel and Glover, 1988). The lack of an identifiable *Rec8* homologue in *Drosophila* is suggestive of conservation of cohesin regulation between somatic cells and gametes, and opens up the possibility of using the *Drosophila* RAD21 cohesin in a somatic screen for regulators of chromosome segregation. Additionally RAD21-containing cohesin complexes are involved in meiosis in other species.

Drawing on the initial studies undertaken by Keall (2005), this metazoan model of chromosome missegregation has been utilised to identify novel modifiers of chromosome cohesion and segregation. By using a system of excessive cohesion it was hoped that genes able to reduce cohesion would be identified and that these genes would form a plausible shortlist of genes that may act as risk factors for loss of cohesion and aneuploidy in humans. Defective chromosome cohesion is a risk factor for chromosome missegregation and aneuploidy in MI, MII and mitosis. The following chapters describe characterisation of the GMR>*Rad21*^{NC} mutant, a genome wide modifier screen to identify metazoan-specific chromosome cohesion regulators, the identification of 133 modifying loci at the molecular level and refinement of this modifier list using secondary assays.

CHAPTER 2:
MATERIALS AND METHODS

2.1 GENERAL LABORATORY CONSUMABLES

2.1.1 General laboratory chemicals

All chemicals used were of analytical grade and were obtained from the following companies: Sigma, Sigma-Aldrich, ProSciTech, MP Biomedicals, Spectrum, Univar, Calbiochem, Amresco, Fluka and Lancaster. Distilled water was obtained using a Barnstead Nanopure Type I ultrapure water system.

2.1.2 Commonly used solutions

- Tris-Acetate EDTA (TAE): 40mM Tris, 20mM acetate, 2mM EDTA, pH 8.1
- Tris-EDTA (TE): 10mM Tris-HCl, pH7.5, 1mM EDTA
- 1X PBS: 140mM NaCl, 3mM KCl, 2mM KH_2PO_4, 10mM Na_2HPO_4
- 1X PBT: 1X PBS, 0.1% Triton X-100
- Luria-Bertani broth (LB): 1% tryptone, 0.5% yeast extract, 1% NaCl, pH 7
- LB with ampicillin (LBA): LB, 75µg/mL ampicillin
- LB plates: LB plus 1.5% agar
- Resuspension Solution: 50mM Tris-HCl, 10mM EDTA, 100µg/mL RNase A, pH 7.5
- Lysis Solution: 1% SDS, 0.2M NaOH
- Neutralisation Solution: 1.32M potassium acetate, pH 4.8
- DNA Binding Solution: 1.5g celite [Diatomaceous Earth, Sigma] suspended in 100mL 7M Guanidine HCl pH 5.5
- Wash Solution: 80mM potassium acetate, 8.3mM Tris-HCl pH 7.5, 40µM EDTA, 50% ethanol.

2.1.3 DNA modifying enzymes

All DNA restriction and modification enzymes were purchased through Promega Corporation or New England Biolabs. Enzymes were used in accordance with the manufacturers' recommendations and/or used in standard procedures described in Sambrook and Russell (2001).

2.2 GENERATION OF PLASMIDS

2.2.1 Minipreparation of plasmid DNA

All minipreparations of plasmid DNA were performed using a modified alkaline lysis method with laboratory-made solutions and Wizard Spin Columns (Promega). Overnight cultures in 1.5 or 3mL of LBA medium were pelleted microcentrifuged at 6,500 x g for 3 mins. Bacterial pellets were resuspended in 200µL of Resuspension Solution. Bacterial cells were lysed by addition of 200µL of Cell Lysis Solution and within 5 mins this reaction was neutralised by the addition of 200µL of Neutralisation Solution. The precipitated proteins, chromosomal DNA and SDS were then pelleted by microcentrifugation at 15,400 x g for 10 minutes. The supernatant was combined with 1mL of DNA Binding Solution and the solution pulled through a Wizard Spin column (Promega) using a vacuum manifold. Columns were then washed with 3mL or more of Wash Solution. Excess ethanol was removed by centrifuging the columns at 4,400 x g for 60 seconds followed by a brief air-drying (5 minutes). Plasmid DNA was then eluted from the column by applying 15-60µL of Tris-EDTA (TE pH7.4) buffer and centrifuging at 6,500 x g for 1 minute.

2.2.2 Large-scale preparation of plasmid DNA

Large-scale plasmid DNA preparations were performed with 25mL or 100mL using the Qiagen Midiprep Kit according to manufacturer's recommendations. Plasmid DNA was eluted using 300µL or 1mL of TE, respectively.

2.2.3 Preparation of **Drosophila** *genomic DNA from single flies*

Genomic DNA was prepared from single flies after euthanasing by freezing in a 1.5mL microfuge tube. A 200µl pipette tip containing 30µl of "squishing" buffer (1mM Tris-Cl pH8.2, 1mM EDTA, 25mM NaCl, 200µg/ml Proteinase K) was then used to mascerate the fly for 30 seconds without expelling any of the liquid. The dissociated fly was suspended in the squishing buffer and incubated at room temperature for 20-30 minutes. The Proteinase K was inactivated by heating the sample at 95˚C for 2 minutes. Preparations were stored at 4˚C and typically 1µl was used as template per 10-15µl PCR reaction (Gloor *et al*., 1993).

2.2.4 PCR

PCR reactions were performed using reagents from Promega, Roche and Sigma Proligo. PCR amplifications were performed using the BioRad iCycler and the Eppendor Mastercycler® Personal thermal cyclers. Thermocycling programs were designed based on optimisation of the following basic parameters:

Table 2.1: Thermocycling parameters

Step	Temperature	Time	Cycles
Denaturation	95˚C	20 seconds	25-30
Annealing	5˚C less than Tm of primers	10 seconds	
Elongation	72˚C	1 minute/kb	
Final elongation	72˚C	10 minutes	1

Table 2.2: Oligonucleotides used in this study

Number	Identifier	Primer sequence (5'-3')
1	DradORF	GACTAGTTGAACATGTTCTATGAGCACA
2	DradM	GCCTGGTTCTCGATTGGATG
3	DradJ	TCGTCTTCAAAAAGGGCTGGT
4	DradL	GCTCTTTTGATACAATCTCCACAGA
5	p35-F	CGGTAGAAATCGACGTGTCC
6	p35-R	ACTCGTAAAGTCCCGTGTCG

Table 2.3: PCR reagents and concentrations

Reagent	Source	Working concentration
GoTaq Polymerase	Promega	1.5U
5x GoTaq Buffer	Promega	1x
dNTPs (2mM)	Roche	0.2mM
$MgCl_2$ (25mM)	Roche	1.88mM
Primers (30µM)	Sigma Proligo	0.45µM
dH_20	Laboratory Nanopure dH_20	Volume to 20µL

2.2.5 Agarose gel electrophoresis

Agarose gels were made using 1x Tris-Acetate-EDTA (TAE) buffer (40mM Tris-acetate, 20mM sodium acetate, 1mM EDTA, pH8.2), 1-2% Molecular Biology Grade Agarose (Spectrum) and supplemented with 50µg/ml ethidium bromide. DNA samples were mixed with an appropriate volume of 6x loading dye prior to loading into wells and run alongside Lamda DNA digested with *Hind*III/*Eco*RI (Promega) as a size marker. Gel electrophoresis was performed in 1xTAE buffer at 100V for 45-60 minutes.

2.2.6 Restriction digest and PCR cleanup

DNA from restriction digests and PCRs intended for use in cloning were purified using Qiagen's QIAquick Gel Extraction Kit or MinElute PCR Purification Kit. Both kits were used in accordance with the manufacturer's recommendations.

2.2.7 Ethanol precipitation of DNA

DNA was precipitated where necessary using 1/10 volume of sodium acetate (3M NaOAc pH5.2) to 1 volume of DNA solution, followed by addition of 2 volumes of cold 100% ethanol. Following incubation on ice for 30 minutes, samples were centrifuged at 4˚C for 15 minutes at 15,000 x g. After discarding the supernatant the DNA pellet was washed with 200µL of 70% ethanol, centrifuged at 4˚C for 5 minutes at 15,000 x g and left to air dry. Finally the pellet was resuspended in 20µL of Tris-EDTA buffer.

2.2.8 DNA ligation

Ligation reactions were set up using a 3:1 molar ratio of insert DNA:vector DNA using the following protocol, where X and Y indicate volumes that vary according to DNA concentration:

T4 DNA ligase (Promega)	1µL
10X Ligase Buffer	1µL
Insert DNA	XµL
Vector DNA	YµL
ddH^20	ZµL (where Z = 8-(X+Y))
TOTAL	10µL

2.2.9 Preparation and transformation of competent bacterial cells

Escherichia coli DH12S cells (80d*lac*ZΔM15 *mcr*A Δ(*mrr-hsd*RMS-*mcr*BC) *ara*D139 Δ(*ara*, *leu*)7697 *lac*X74 *gal*U *gal*K *rps*L (Str^R) *nup*G *rec*A1/F' *pro*AB^+ *lac*$I^qZ\Delta M15$) were made competent using the cold calcium chloride preparation technique as described in Protocol 25, section 1.116-1.117of Sambrook and Russell (2001). Transformation of competent bacterial cells was carried out following the heat shock technique described by Sambrook and Russel (2001).

2.2.10 DNA sequencing

All DNA sequence analysis was performed by Macrogen Inc, Korea, using primers listed in table 2.2. Template DNA was dried down using ethanol precipitation at 0.5-1µg per reaction and primers were individually dried down at 50pmoles per reaction prior to shipping to the sequencing facility. Sequencing was performed using the BigDye™ terminator cycling conditions and run using Automatic Sequencer 3730xl.

2.3 GERM-LINE TRANFORMATION OF *DROSOPHILA MELANOGASTER*

2.3.1 Microinjection of Drosophila *embryos*

Injection mixes were created by co-precipitating pUAST-derived recombinant plasmid constructs with pπ25.7wc (Δ2-3 helper transposase) and resuspending in 1x injection buffer (5mM KCl, 0.1mM PO_4 pH7.8) to give a final concentration of 1µg/µL for each plasmid. Particulate matter was removed from the mix by centrifuging at 15,400 x g for 5 minutes just prior to loading the injection needle. DNA was delivered to embryos via an Eppendorf Femptojet microinjector with injection needles pulled from 1mm thin-walled borosilicate glass capillaries was used for volume-controlled injection of embryos.

W^{1118} embryos were collected in ½ hourly batches from cages of 1-7 day old adults maintained on 2% grape-juice agar plates supplemented with live yeast paste. An Olympus SZ60 dissecting microscope was used to assist manual dechorionation of 300+ w^{1118} embryos for each injection session. Dechorionated embryos were

arranged side-by-side on a glass slide using a strip of low-toxicity double-sided tape (3M) for adhesion. Embryos were dehydrated for 5-10 minutes before being covered with Halocarbon 700 oil (Sigma). A small quantity of injection mix was injected into the posterior cytoplasm of each embryo. Following injection, slides of embryos were incubated at in an oxygen enriched chamber at room temperature for 24 hours to promote development. Larvae were removed from the slide to vials of standard cornmeal treacle medium supplemented with Instant *Drosophila* media (Sigma) at a density of 25-35 larvae per 30mL vial.

2.3.2 Identification of transgenic flies and mapping of insertions

All G_0 adult flies were individually back crossed to several w^{1118} flies to allow identification of germline transformants in the G_1 generation on the basis of inheritance of the w^+ eye pigmentation marker carried by the pUAST constructs. Using G1 flies with pigmented eyes were collected and individually crossed to flies carrying both second and third chromosome balancer chromosomes (If/CyO; MKRS/TM6B) with dominant phenotype markers. G_2 flies bearing second and third balancer chromosome markers and pigmented eyes were backcrossed to w^{1118} stock and segregation analysis used to assess the chromosomal linkage of insertion site of the transgene.

2.4 *DROSOPHILA MELANOGASTER* CULTURING

2.4.1 Drosophila *stocks and maintenance*

Drosophila stocks used in this study were sourced primarily from Bloomington Stock Center, Indiana University. Other stocks were sourced from the Vienna *Drosophila* RNAi Centre (VDRC) or from other *Drosophila* laboratories. All stocks used in this study are listed in Appendices 1-5. All cultures used in this study were maintained at 18ºC, 25ºC or 29ºC on standard cornmeal-treacle medium. All crosses, except for the GMR-Gal4 overexpression phenotype crosses, were performed at 25ºC. All fly work was performed using CO_2 to temporarily anaesthetise flies and an Olympus SZ60 dissecting microscope with an Olympus LG-PS2 fibre-optic light source was used for viewing.

2.4.2 Generation of recombinant stocks

The GMR>UAST-RAD21^{NC},UAS-p35/CyO stock was generated via meiotic recombination. Separate stocks carrying GMR>UAST-RAD21^{NC} and UAS-p35 transgenes on the second chromosome were crossed and heterozygous female flies carrying GMR>UAST-RAD21^{NC}/UAS-p35 were selected and crossed to If/CyO males. Recombinant progeny were identified by phenotypic suppression of the RAD21^{NC} rough-eye phenotype by p35 in the presence of curly wings. Diagnostic PCR was performed using p35 specific primers (Table 2.2) to confirm the presence of the p35 transgene.

2.5 SDS-PAGE AND WESTERN BLOTTING

2.5.1 Protein expression

In vivo protein expression was driven using the Gal4-UAS system, using either the eye-specific GMR-Gal4 driver (P{GAL4-ninaE.GMR}) or a ubiquitous heat shock-Gal4 driver (TM3(hs-Gal4, UAS-EGFP – see Appendix 1). Protein samples were collected by dissecting eye-antennal imaginal discs from actively wandering third instar larvae or adult heads after larvae and adults had been washed in series in tap water, 70% ethanol and distilled water. Imaginal discs were dissected in 1xPBS (7.5mM Na_2PO_4, 2.5mM NaH_2PO_4, 145mM NaCl) before being transferred to cold protein sample buffer or adult heads were removed using a clean scalpel before being transferred to cold protein sample buffer. The tissues were disrupted using a pestle before boiling at 95˚C for 10 minutes, followed by centrifugation at 4˚C at 17,500 x g for 15 minutes. The supernatant was transferred to a fresh chilled 1.5mL microfuge tube and re-centrifuged at 4˚C at 17,500 x g for 15 minutes. The supernatant was again transferred to a fresh chilled 1.5mL microfuge tube and either used immediately or snap frozen in liquid nitrogen and stored at -20˚C for up to 2 weeks.

2.5.2 SDS-PAGE and protein transfer

Proteins were separated on 10% acrylamide gels at 100V for 1.5 hours in 1xRunning Buffer (25mM Tris, 192mM glycine, 0.1% v/v SDS) at room temperature in a MiniProtean3 electrophoresis system (BioRad). The same system was used with an

ice block to maintain room temperature when samples were transferred to a Trans-Blot nitrocellulose membrane (BioRad) by wet electroblotting at 100V 0.35A for 1.5 hours in 1xTransfer Buffer (25mM Tris, 192mM glycine, 0.5% v/v SDS, 10% v/v methanol). The nitrocellulose membrane was prepared by soaking in transfer buffer for 5 minutes prior to use.

2.5.3 Protein detection

Transfer membranes were blocked, typically overnight, in 8% skim milk powder, 1% BSA and 1% fish skin gelatin (FSG) in 1xTBS. Following a quick rinse in 1xTBS, 0.5% Tween-20 (1xTBS-T), the membrane was incubated overnight with the primary antibody in antibody solution (0.5% BSA, 0.5% FSG in 1XTBS-T) at 4˚C. Membranes were washed four times for ten minutes each wash in 1xTBS, 0.5% Tween-20, prior to being incubated for a minimum of two hours with the secondary antibody in antibody solution. After washing four times for ten minutes in 1xTBS-T, membranes were incubated with ECL reagents for one minute and then exposed to X-ray film (Kodak BioMax Light) for a variable amount of time. Films were developed using a Kodak X-OMAT 1000 processor.

Table 2.4: Antibodies used for Western Blots

Antibody	Source	Working Concentration
Rat anti-Scc1 (1˚)	Sunkel Laboratory	1:250
Rat anti-HA (1˚)	Roche	200ng/µL
Goat anti-rat-HRP (2˚)	Zymed Laboratories	1:5000

2.6 EYE-ANTENNAL IMAGINAL DISC STAINING

2.6.1 Immunofluorescence

Eye-antennal imaginal discs were dissected from 3rd instar larvae in 1xPBS, keeping the mouthparts attached for ease of manipulation. Dissected tissues were fixed in fresh 3.7% paraformaldehyde (in PBS) for 45 minutes. The tissues were washed briefly (5 minutes) in 1xPBT, prior to washing with antibody wash solution (1xPBS,

0.2% BSA, 0.1% Triton X-100) for 30 minutes. The tissues were blocked in antibody block solution (1xPBS, 1% BSA, 0.3% Triton X-100, 10% donkey serum, 1mg/mL RNase A) for at least one hour prior to incubation with the primary antibody in fresh block solution overnight at 4˚C. Discs were washed with antibody wash solution and incubated with the secondary antibody for two hours at room temperature. Finally the discs were washed with antibody wash solution, during which time the extraneous material was removed from the eye discs by careful dissection and discarded. Discs were then mounted on glass slides in 80% glycerol 0.5M EDTA and sealed under glass coverslips using clear nail varnish.

Table 2.5: Antibodies used for immunofluorescence

Antibody	Source	Working Concentration
Rabbit anti-phospho-histone H3 (1˚)	Upstate Biotechnology	1:2000
Goat anti-rabbit Alexafluor-488 (2˚)	Molecular Probes	1:2000

2.6.2 Acridine orange staining

Eye-antennal imaginal discs were dissected from 3rd instar larvae in 1xPBS, keeping the mouthparts attached for ease of manipulation. The dissected tissues were then transferred to a drop of acridine orange stain (Sigma: 1µg/mL in 1xPBS) for 5-10 minutes. The eye discs were then transferred to a drop of 1xPBS to wash for at least 5 minutes, while the mouth parts and other extraneous materials were detached from the eye discs and discarded. Stained eye discs were mounted on glass slides in 1xPBS, using Cellotape as a support bridge to prevent the coverslips from squashing the unfixed discs. Discs were immediately viewed using an Olympus BX51 epifluorescence microscope with a GFP filter and images captured using an Optronics MagnaFire digital camera.

2.7 ANALYSIS OF ADULT WINGS

2.7.1 Preservation and mounting

Whole flies were collected and preserved in a solution of 50:50 lactic acid:ethanol for a minimum of 24 hours (and up to three weeks). Under a dissecting microscope, the wings were then removed using Dumont No.5 Inox tweezers and mounted flat on a glass slide in preservation solution. Coverslips were sealed over the wing samples using clear nail varnish.

2.7.2 Image capture and analysis

Images were captured using brightfield microscopy on an Olympus BX51 and Optronics MagnaFire digital camera. Once collected, the images were individually analysed to determine the number of pixels in the wing blade area (red section of Figure 2.1) using Adobe Photoshop CS2. The wing blade area was analysed as the hinge region (blue area of Figure 2.1) is not influenced by vg-Gal4 driven expression. The wing blade area was selected and the hinge region excluded based on the wing notch landmarks (Figure 2.1).

2.7.3 Wing image analysis

GMR>UAST-*Rad21*^{NC} modifier alleles were crossed to the vgMQ-Gal4>UAST-*Rad21*^{NC}*-2HA* stock followed by collection of test and control progeny wings for measurement of wing blade area. Data from each experimental group was statistically compared to a sibling control group using a Students' Unpaired T-test, following normalisation of the data. For statistical relevance a minimum cohort (N) of 12 wings was analysed for each group, this was determined using a nomogram (Figure 2.2) designed to calculate sample size based on standardised difference and power. Based on preliminary data, the physically relevant difference between samples was determined to be 26,500 pixels and the standard deviation was calculated at 23,000 pixels. Therefore, the standard difference (Δ_s) = relevant difference (δ) / estimated standard deviation (s), was calculated as 1.2. To achieve a power of 80% a total sample size of 24 was required with 12 (N/2) samples for the experimental and control groups. This, however, was an arbitrary number and being a biological system test and control groups were not always equal in number, which required a slight adjustment to the total sample size (N' = 25, N/2 = 12.5) to maintain

a power of 80% (Whitley and Ball, 2002). Due to poor *Drosophila* viability this sample quota was not always met for every cross and where this was the case the results have been dealt with separately to take into account the reduced power of these data.

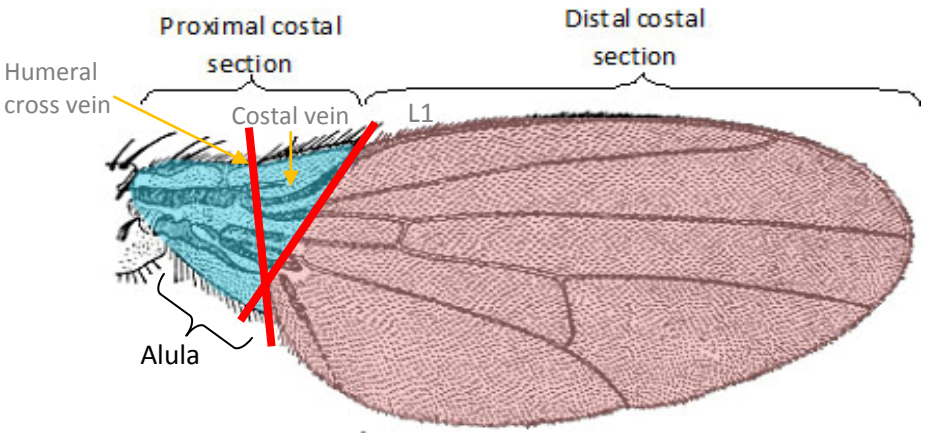

Figure 2.1: Dorsal aspect of adult wing with landmarks. Notches in wing margin indicate the boundary between the wing hinge and wing blade. The red lines transect at selected wing landmarks and indicate the boundary between the hinge and blade regions. The notch between the proximal costal section and the distal costal section coincides with the termini of wing vein L1 and the costal vein. The notch in the middle of the proximal costal section coincides with humeral cross vein. Both lines transect the alula proximally. (Figure adapted from Biology of *Drosophila*, 1994).

2.8 MICROSCOPY

2.8.1 Confocal microscopy

All confocal microscopy was carried out using a BIO-RAD Radiance 2000 laser scanning confocal microscope and images captured using BioRad LaserSharp2000 software.

2.8.2 Scanning electron microscopy (SEM)

Adult flies were prepared for SEMs by anaesthetisation with CO_2 before being transferred to 25% ethanol. The flies were dehydrated by sequentially increasing the ethanol content to 50%, 75% and 100% and left at each of these stages for a minimum of 24 hours. The 100% step was repeated three times. When fully dehydrated, the flies were incubated in a 1:1 mix of hexamethyldisilasane (HMDS) and ethanol for 10 minutes. This was followed by incubation in 100% HMDS for 10 minutes and repeated three times. Flies were quick dried on Whatman 3MM filter paper in and then transferred to 4ºC overnight to allow slow drying of the samples. All steps prior to the drying at 4ºC involving HMDS were performed in the fumehood for safe ventilation of fumes.

Fly samples were mounted onto stubs with adhesive circles prior to sputter coating with 5 or 6 layers of either gold or platinum (performed by Dr. Kevin Blake or Shane Askew using a JEOL sputter coating machine). The coated samples were then analysed using a JEOL (JSM-541-LV) scanning electron microscope and the Semaphore digital imaging system.

CHAPTER 3: ANALYSIS OF THE *DROSOPHILA* RAD21 MODEL

3.1 INTRODUCTION

In the study of chromosome cohesion and chromosome dynamics that depend on this cohesion, two obvious strategies for developing a model are decreasing cohesion and increasing cohesion. In the absence of knowledge of the chromosomal location for *Rad21* and any known mutants that could be used as models of reduced chromosome cohesion at the time of commencing this study, an alternative option was increasing cohesion by developing and ectopically expressing a "non-cleavable" cohesin variant. An additional feature of the non-cleavable cohesin model is that cleavage occurs at a very specific time in the cell cycle and therefore phenotypes produced and genetic interactions with these phenotypes can be temporally pinpointed. In order to truly understand and hypothesise on the genetic interactions uncovered by a genetic screen, the aetiology of the mutant phenotype needs to be thoroughly characterised.

This chapter describes the approaches used to generate and characterise a collection of epitope-tagged *Rad21* transgenics. The $Rad21^{NC}$ allele was pursued as a mechanism for identifying modifiers of chromosome cohesion and in particular, modifiers that could weaken chromosome cohesion. However, it remained to be conclusively demonstrated that the proteolytic cleavage pattern of these mutated RAD21 proteins is altered from that of wildtype RAD21 when expressed in *Drosophila* eye cells. It was also unclear whether incorporation of $RAD21^{NC}$ into functional cohesin complexes was preventing the segregation of the replicated chromosomes at the cellular level and what the resulting cellular responses to and consequences of inhibited chromosome segregation in this way may be.

Although Keall (2005) had clearly demonstrated that mitotic arrest and apoptosis were significant factors underlying the final GMR>$Rad21^{NC}$ eye phenotype questions remained regarding the extent of the influence of these factors. Particularly, was the overexpression of RAD21 alone influencing eye development? Could the transgene expression be influenced through modulation of the driver? Also, introduction of a single copy of cDNA encoding the anti-apoptotic baculovirus p35 protein strongly suppressed the GMR>$Rad21^{NC}$ eye phenotype. Therefore, would increasing the level of p35 further increase the suppression of the phenotype

towards wildtype? This chapter describes attempts used to directly and indirectly determine the consequences of expressing *Rad21* and various mutant forms of *Rad21* in the developing eye under the control of GMR-Gal4.

3.2 RESULTS

3.2.1 Generation and expression of Rad21-HA transgenics

3.2.1.1 Generation of Rad21-HA *variants*

In order to express transgenic RAD21 proteins that could be distinguished from endogenous RAD21, transgenic *Drosophila* were generated that could express *Rad21* protein tagged with two tandem copies of the haemagglutinin (HA) epitope positioned at the carboxy-terminus. The untagged Rad21 variants generated previously by Keall (2005) had provided inconclusive results when utilised for Western Blot analyses. Tagging of the *Rad21* and *Rad21*^{NC} constructs was carried out by Dr. Kylie Gorringe by cutting the *Rad21* cDNA sequence using *Bst*BI (Figure 3.2A), followed by ligation with overlapping oligonucleotides containing the HA coding sequence. Single tagged mutants, *Rad21*^{N}-2HA and *Rad21*^{C}-2*HA*, were later generated through a "cut and paste" scheme using the *Rad21*-2*HA* and *Rad21*^{NC}-2*HA* constructs (Figure 3.2B). The presence of the cleavage-site amino acid substitutions was confirmed by analysing the constructs for restriction sites introduced by the original site-directed mutagenesis that altered the Separase cleavage site sequences. An *Sph*I restriction site introduced at the amino-terminal Separase cleavage site in the R175A alleles, and an *Nae*I restriction site introduced in the sequence encoding the carboxy-teriminal Separase cleavage site RA474AG (Figure 3.2A) aided molecular analyses. Following subcloning into P-element vector pUAST, *Nae*I/*Sph*I double digests of the pUAST-*Rad21*-2*HA* constructs produced the expected restriction fragments, demonstrating the presence of the desired mutations (R175A/RA474AG) (Figure 3.2, Table 3.1 and Figure 3.3). DNA sequencing analyses were performed to further confirm the presence of the HA tag sequence and that the integrity of the cDNA sequence had not been compromised. Independent transgenic *Drosophila* lines were generated with the four different *Rad21*-2*HA* constructs (Table 3.2), via microinjection of construct DNA into *Drosophila*

embryos, as described in section 2.3.1. The transgene insertion sites were mapped by segregation analysis for all independent transgenic lines, as shown in Table 3.2.

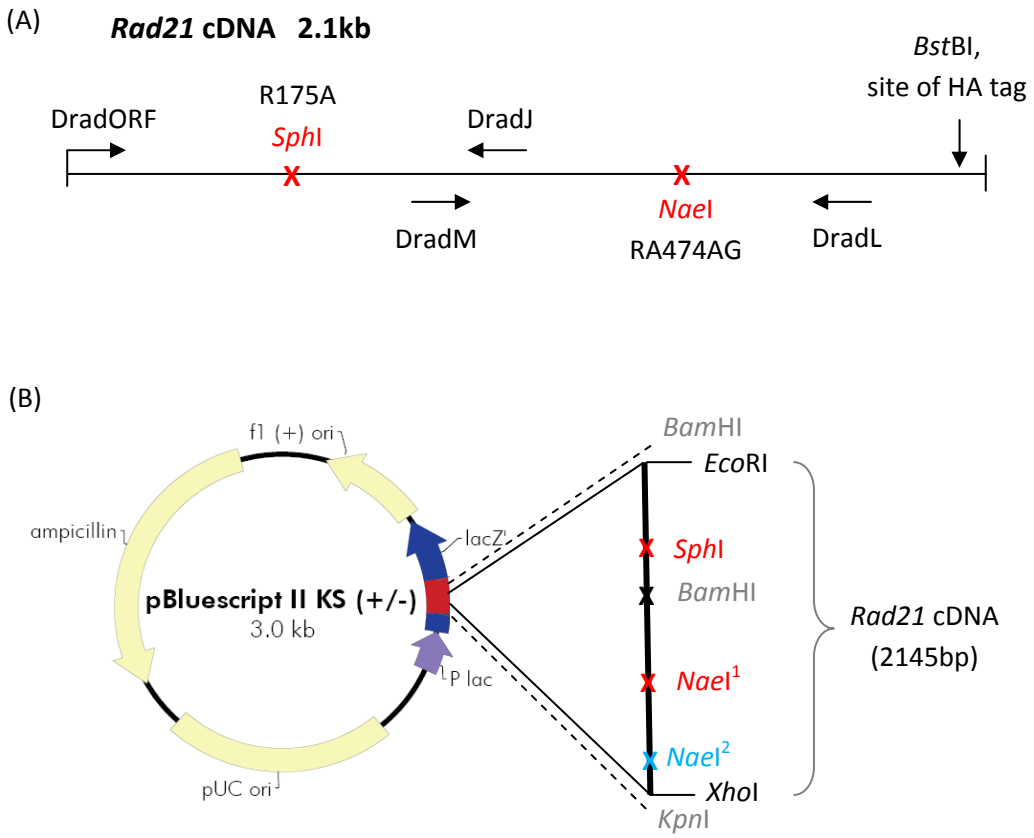

Figure 3.1: The *Rad21* plasmid constructs. (A) Schematic of the d*Rad21* cDNA with amino- and carboxy-terminal sequence changes with introduced restriction sites, primer binding sites and the site of the introduction of the HA tags. (B) Restriction map of the pBluescript KS+-*Rad21*-2*HA* construct. The *Eco*RI, *Bam*HI and *Xho*I sites were used in the "cut and paste" scheme to generate the *Rad21*^{N}-2*HA* and *Rad21*^{C}-2*HA* single mutants. The *Eco*RI and *Kpn*I sites were used to sub-clone Rad21-2HA into the P-element vector pUAST. A second *Nae*I site (*Nae*I^{2}) was introduced with the HA tag sequence and the *Nae*I and *Sph*I sites were used for confirmation digests (Figure 3.2). (Image adapted from Stratagene pBluescript II Phagemid Vectors Instruction Manual).

Table 3.1: Expected band sizes for *Sph*I/*Nae*I double digests of the pUAST-*Rad21*-2*HA* constructs (based on the *Rad21* restriction map in Figure 3.1)

Construct	pUAST-*Rad21-2HA*	pUAST-*Rad21*^{N}-*2HA*	pUAST-*Rad21*^{C}-*2HA*	pUAST-*Rad21*^{NC}-*2HA*
*Nae*I^{3}-*Nae*I^{1}	10,000bp	10,000bp	10,000bp	10,000bp
*Nae*I^{1}-*Nae*I^{3}	2600bp			
*Sph*I-*Nae*I^{3}		1675bp		
*Nae*I^{1}-*Sph*I		925bp		
*Nae*I^{1}-*Nae*I^{2}			1822bp	
*Nae*I^{2}-*Nae*I^{3}			778bp	778bp
*Nae*I^{1}-*Sph*I				925bp
*Sph*I-*Nae*I^{2}				897bp

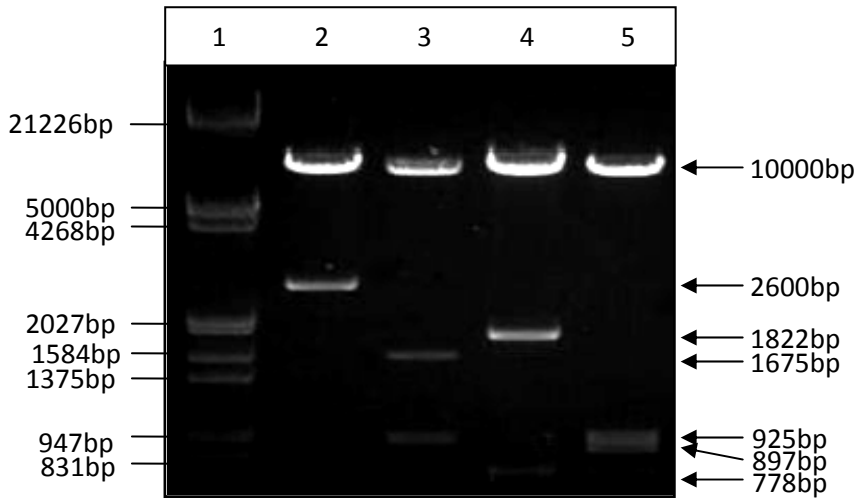

Figure 3.2: Confirmation digests of pUAST-*Rad21-2HA* constructs. *Nae*I/*Sph*I double digests of pUAST-*Rad21*-2*HA* (lane 2), pUAST-*Rad21*^{N}-2*HA* (lane 3), pUAST-*Rad21*^{C}-2*HA* (lane 4) and pUAST-*Rad21*^{NC}-2*HA* (lane 5). Lane 1 contains 0.75 µg of λ *Hind*III/*Eco*RI DNA ladder (Promega).

Table 3.2: *Rad21*-2*HA* transgenic lines			
Construct	**Independent transgenic lines**	**Line identifier**	**Chromosome mapped to**
pUAST-*Rad21*-2*HA* (*Rad21*-2*HA*)	5	5	2
		14.2	3
		14.11	X
		28.2	2
		28.3	3
pUAST-*Rad21*^{R175A}-2*HA* (*Rad21*^{N}-2*HA*)	2	A	2
		R	X
pUAST-*Rad21*^{RA474AG}-2*HA* (*Rad21*^{C}-2*HA*)	9	B	2
		C	ND
		E	3
		F	3
		G	3
		H	2
		I	3
		J	2
		K	X
pUAST-R*ad21*$^{R175A/RA474AG}$-2*HA* (*Rad21*^{NC}-2*HA*)	8	4	3
		6	X
		14	ND
		A	ND
		H	2
		P	ND
		O	2
		XA	X

3.2.1.2 Ectopic expression of Rad21-HA *variants*

The eye-specific driver P{GAL4-ninaE.GMR} (referred to from here as GMR-Gal4 or GMR>) was used to drive expression of the transgenes in the photoreceptor cells of the developing larval eye imaginal disc. In the adult compound eye the RAD21-2HA, RAD21^{N}-2HA and RAD21^{C}-2HA proteins did not produce an abnormal phenotype. In contrast the RAD21^{NC}-2HA protein produced an eye phenotype that was significantly reduced in overall size and ommatidial organisation compared to wildtype or eyes expressing the other HA-tagged RAD21 proteins (Table 3.4; Figure 3.3).

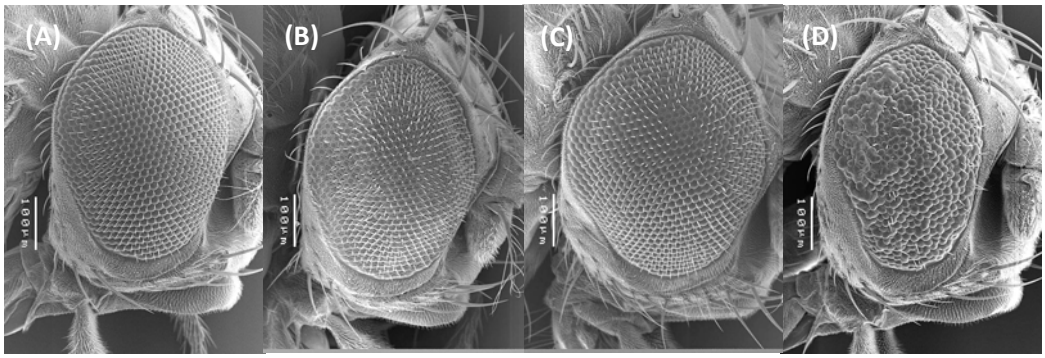

Figure 3.3: Ectopic expression of RAD21-2HA variants. The phenotype of the adult eye expressing (A) UAST-*Rad21-2HA* (line 5), (B) UAST-*Rad21^{N}-2HA* (line R), (C) UAST-*Rad21^{C}-2HA* (line H) and (D) UAST-*Rad21^{NC}-2HA* (line H) under the control of GMR-Gal4. Expression of the RAD21^{NC}-2HA protein produced an eye phenotype that was significantly reduced in overall size and ommatidial organisation (D). No variation was observed for independent transgenic lines of wildtype *Rad21* or single mutants (R175A and RA474AG. Only slight variation of the level of eye disorganisation was observed for the different independent *Rad21^{NC}* transgenic lines tested, presumably due to transgene insert-site effects on expression levels.

3.2.2 Generation and expression of Rad21-GFP *transgenics*

3.2.2.1 Generation of Rad21-GFP *variants*

It remained to be determined whether a GFP epitope tag did in fact prevent functional cohesin complexes from forming, as had been previously speculated following failure of pUAST-*Rad21^{C}-GFP* transgenics to produce an expected rough-eye phenotype when expression was driven by GMR-Gal4. This followed on from data that indicated an untagged pUAST-*Rad21^{C}* transgene produced a rough-eye phenotype when driven by GMR-Gal4. Previous studies using wildtype *Drosophila Rad21* tagged with GFP demonstrated that it was localising to the chromosomes in a pattern consistent with endogenous cohesin, which indicated that the RAD21-GFP protein was at least localising normally. P-element constructs for *Rad21-GFP*, *Rad21^{N}-GFP*, *Rad21^{C}-GFP* and *Rad21^{NC}-GFP* had been generated previously (Keall, 2005) by cloning wildtype and mutant (R17A and RA474AG) cDNAs inframe with EGFP coding sequences from pALX190, then subcloning the *Rad21-GFP* fragment into pUAST. Transgenic flies existed for the *Rad21-GFP* and *Rad21^{C}-GFP* constructs and so to confirm the hypothesis that GFP was not blocking cohesin complex formation, the *Rad21^{N}-GFP* and *Rad21^{NC}-GFP* transgenics were also generated (Table 3.3). A total of six independent transgenic lines were generated for the pUAST-R*ad21*^{R175A}*-GFP* construct and two independent trangenic lines for the pUAST-R*ad21*$^{R175A/RA474AG}$*-GFP* construct, with each of these insertions being mapped via chromosome segregation analysis (Table 3.3).

Table 3.3: *Rad21-GFP* transgenic lines

Construct	Independent transgenic lines	Line identifier	Chromosome mapped to
pUAST-R*ad21*^{R175A}*-GFP* (*Rad21^{N}-GFP*)	6	M	2
		N	3
		O	3
		P	3
		S	2
		T	3
pUAST-R*ad21*$^{R175A/RA474AG}$*-GFP* (*Rad21^{NC}-GFP*)	2	L	3
		Q	3

3.2.2.2 Ectopic expression of Rad21-GFP *variants*

Ectopic expression of $RAD21^{WT}$-GFP, $RAD21^{N}$-GFP and $RAD21^{C}$-GFP under the control of GMR-Gal4 resulted in normal eye development, whereas ectopic expression of $RAD21^{NC}$-GFP produced a severely reduced and disorganised eye phenotype (Figure 3.4, Table 3.4). The expression of the RAD21-GFP fusion protein was confirmed by epifluorescence microscopy (data not shown). The ability of $RAD21^{NC}$-GFP to produce a phenotype equivalent to that produced by untagged and HA tagged $RAD21^{NC}$ indicates that GFP-tagging of RAD21 does not prevent functional incorporation of this subunit into the cohesin complex. This also indicated that the original analysis deeming the *Drosophila* carboxy-terminal Separase cleavage site to be the dominant site of cleavage was inconsistent with previous data, suggesting that this conclusion may require further investigation (see section 3.2.5).

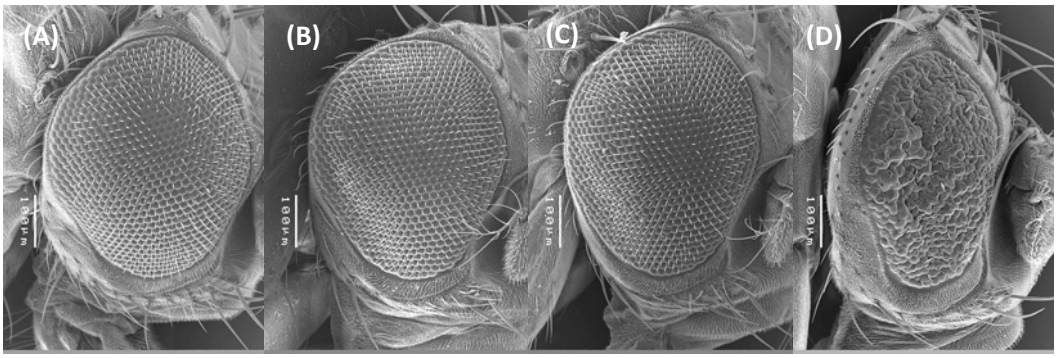

Figure 3.4: Ectopic expression of RAD21-GFP variants. (A) GMR>UAST-*$Rad21^{WT}$-GFP* (line N2A, Keall 2005), (B) GMR>UAST-*$Rad21^{N}$-GFP* (line O), (C) GMR>UAST-*$Rad21^{C}$-GFP* (line 19-2, Keall 2005) and (D) GMR>UAST-*$Rad21^{NC}$-GFP* (line L). The *$Rad21^{WT}$-GFP*, *$Rad21^{N}$-GFP,* and *$Rad21^{C}$-GFP* mutants (A-C) show no obvious eye abnormalities when expressed under the control of GMR-Gal4, while the *$Rad21^{NC}$* double-mutant (D) displays a rough-eye phenotype very similar to that observed with untagged *$Rad21^{NC}$*. No variation was observed for independent transgenic lines of wildtype *Rad21* or single mutants (R175A and RA474AG. Slight variation of the level of eye disorganisation was observed for independent transgenic lines expressing *$Rad21^{NC}$*.

Table 3.4: *Rad21* variant phenotypes observed			
Construct	**Tag**	**Eye phenotype with GMR-Gal4 driver**	**Reference**
pUAST-*Rad21* (*Rad21*)	Untagged	Wildtype	Keall, 2005
	HA-tagged	Wildtype	This study
	GFP-tagged	Wildtype	This study
pUAST-R*ad21*^{R175A} (*Rad21*^{N})	Untagged	Wildtype	Keall, 2005
	HA-tagged	Wildtype	This study
	GFP-tagged	Wildtype	This study
pUAST-*Rad21*^{RA474AG} (*Rad21*^{C})	Untagged	Reduced size and ommatidial organisation[ə]	Keall, 2005
	HA-tagged	Wildtype	This study
	GFP-tagged	Wildtype	This study
pUAST-*Rad21*$^{R175A/RA474AG}$ (*Rad21*^{NC})	Untagged**	Reduced size and ommatidial organisation	Keall, 2005
	HA-tagged	Reduced size and ommatidial organisation	This study
	GFP-tagged	Reduced size and ommatidial organisation	This study

[ə]This abnormal phenotype was later found to be incorrect (see section 3.2.5) and therefore no untagged pUAST-*Rad21*^{C} transgenics exist.

**The independent line 24A of untagged *Rad21*^{NC} transgene recombined with GMR-Gal4 on the 2nd chromosome (Keall, 2005) and balanced over CyO was used for the genome-wide screen and all other *Rad21*^{NC} experiment unless stated that a HA epitope-tagged *Rad21*^{NC} was utilised.

3.2.3 RAD21 variant cleavage patterns

Although Keall (2005) had characterised the gross phenotypic consequences of *Rad21*^{NC} expression, it remained to be demonstrated that mutating the Separase cleavage sites of RAD21 actually resulted in altered RAD21 protein cleavage products. Previous efforts using untagged recombinant RAD21 proteins and Western Blotting to assess cleavage patterns of mutant variants of RAD21 compared to wildtype RAD21 were inconclusive (Keall, 2005). As a result, experiments examining proteolysis of HA-tagged and GFP-tagged RAD21 variants were undertaken to distinguish endogenous and exogenous RAD21 protein signals. HA-tagged transgenic lines yielded a RAD21-HA protein band on Western Blots of approximately 120kD (Figure 3.5) and GFP-tagged transgenic lines yielded a RAD21-GFP protein band 130kD on Western Blots (Figure 3.5), consistent with the phosphorylated full-length form of RAD21. Full length RAD21 was observed in protein samples sourced from RAD21^{WT}-2HA (Figure 3.5A), RAD21^{WT}-GFP (Figure 3.5C), RAD21^{N}-2HA (data not shown), RAD21^{C}-2HA (data not shown), RAD21^{NC} (Figure 3.5C) and RAD21^{NC}-2HA (Figure 3.5B) transgenics.

Despite extensive efforts and numerous attempts, bands for the wildtype RAD21 cleavage products, expected to be 60kD and 27kD for the amino- and carboxy-terminal cleavage products, respectively, were not observed using either anti-HA or anti-Scc1 antibodies. As only a fraction of the total cohesin population in a cell is loaded onto chromosomes and in metazoans the majority of this is removed during the prophase dissociation step, only a few percent of the total cellular cohesin population is proteolytically cleaved by Separase at the onset of anaphase (Hauf *et al*., 2001). By expressing these proteins *in vivo* in the fly eye (driven by GMR-Gal4), or even ubiquitously (driven by hs>Gal4), the population of cohesin being cleaved by Separase at any given time is very small due to the asynchronous nature of the cell divisions

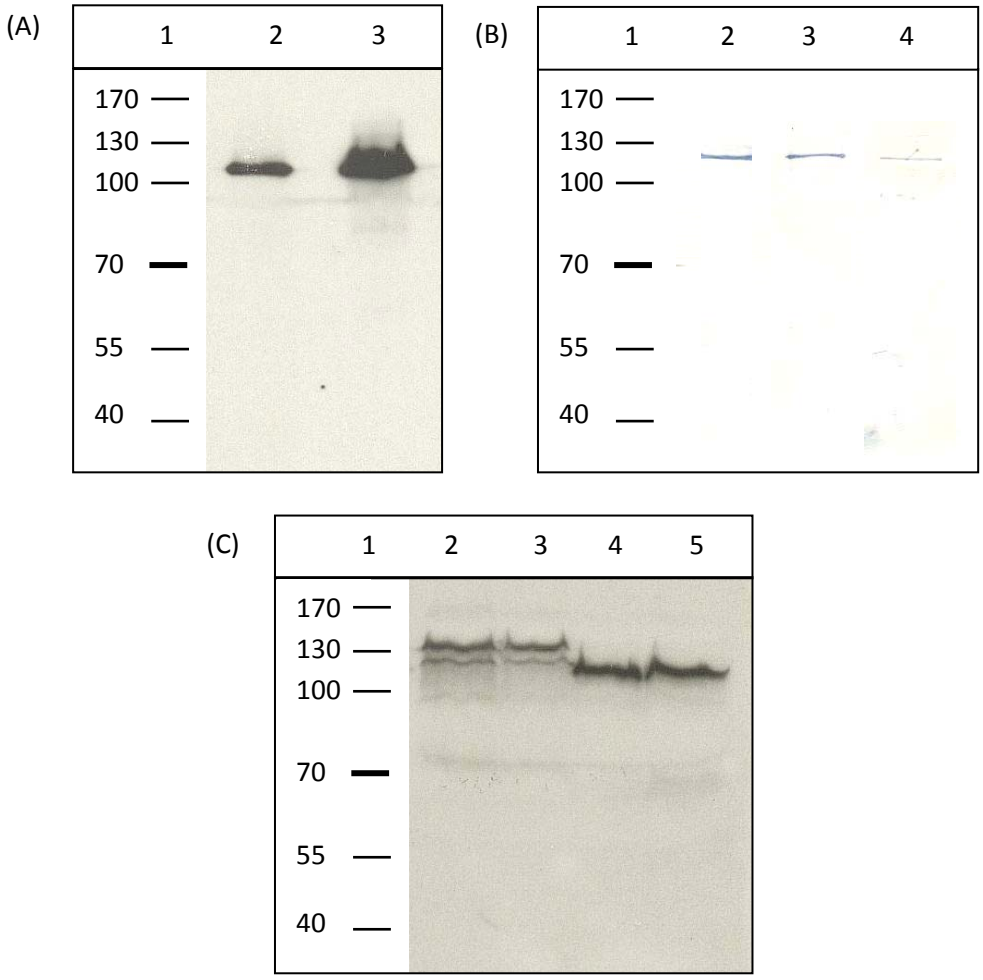

Figure 3.5: Detection of epitope-tagged RAD21 protein by Western Blotting. Blot (A): PageRuler^{TM} (Fermentas)(Lane 1), Protein extract from 6 adult *Drosophila* heads TM3(hs-Gal4),UAS-EGFP/UAST-*Rad21*^{WT}-2*HA*, line 28.3)(Lane 2), and Protein extract from 12 adult *Drosophila* heads TM3(hs-Gal4),UAS-EGFP/UAST-*Rad21*^{WT}-2*HA*, line 14.2)(Lane 3); NB – protein samples were collected 10 hours post heat shock treatment.
Blot (B): PageRuler^{TM} (Fermentas) (Lane 1); samples of 45 eye-antennal imaginal discs: GMR>UAST-*Rad21*^{WT}-2*HA*/CyO (Lane 2), GMR>UAST-*Rad21*^{C}-2*HA*/CyO (Lane 3), GMR>UAST-*Rad21*^{NC}-2*HA*/CyO (Lane 4).
Blot (C): PageRuler^{TM} (Fermentas)(Lane 1), UAST-*Rad21*^{WT}-GFP/+;TM3(hs-Gal4),UAS-EGFP/+ (line J2A) 5 pupae (Lane 2), TM3(hs-Gal4),UAS-EGFP/UAST-*Rad21*^{WT}-GFP (line N2A) 3 pupae (lane 3), TM3(hs-Gal4),UAS-EGFP/UAST-*Rad21*^{NC} 5 pupae (Lane 4), and TM3(hs-Gal4),UAS-EGFP/UAST-*Rad21*^{NC} 12 pupae (Lane 5); NB – protein samples were collected 16 hours post heat shock treatment. Blots were pr.obed using rat anti-HA (Roche) primary antibody and goat anti-rat-HRP (Zymed Laboratories) secondary antibody.

3.2.4 Cleavage-resistant RAD21 cellular phenotypes

RAD21^{NC} had been found to produce a demonstrable deleterious effect on the development of the adult compound eye; however, visualisation of the effects of RAD21^{NC} at the cellular level remained to be definitively demonstrated. In order to achieve this, neuroblast squashes were used to allow visualisation of mitotic chromosomes and analysis of segregation defects. The neuroblast squashes were performed following a heatshock treatment (8 and 16 hours post-heatshock) to induce ubiquitous RAD21^{NC} expression in larvae carrying a heatshock-Gal4 driver and the UAST-*Rad21^{NC}* transgene. The lethality induced by expressing RAD21^{NC} in dividing cells results in this phenotype being extremely difficult to capture and analyse, however, a significant number of neuroblasts from the larval brain had observable chromosomal defects compared to controls (Table 3.5). The observed chromosomal defects were tetraploidy, polyploidy, chromosomal fragmentation and abnormal anaphases, many with lagging chromosomes (Figure 3.6). These phenotypes were almost entirely absent from hs-Gal4 control brain squashes (Table 3.5).

Table 3.5: hs-Gal4>*Rad21^{NC}* neuroblast analysis.

Treatment	Genotype	Diploid	Tetra- or polyploid	Fragments	Anaphase	Total
No heatshock	hs-Gal4 control	554 (86.4%)	1 (0.2%)	0 (0.0)	86 (13.4)	641 (100.0)
	hs-Gal4, *Rad21^{NC}*	622 (87.0%)	0 (0.0%)	0 (0.0)	93 (13.0)	715 (100.0)
Heatshock +8 hours	hs-Gal4 control	505 (81.1%)	0 (0.0%)	0 (0.0)	118 (18.9)	623 (100.0)
	hs-Gal4, *Rad21^{NC}*	403 (79.0%)	13 (2.5%)	14 (2.7)	80 (15.7)	510 (100.0)
Heatshock +16 hours	hs-Gal4 control	725 (87.5%)	2 (0.2%)	0 (0.0)	102 (12.3)	829 (100.0)
	hs-Gal4, *Rad21^{NC}*	678 (66.3%)	199 (19.5%)	64 (6.3)	82 (8.0)	1023 (100.0)

(Data collated by Dr. S. Page)

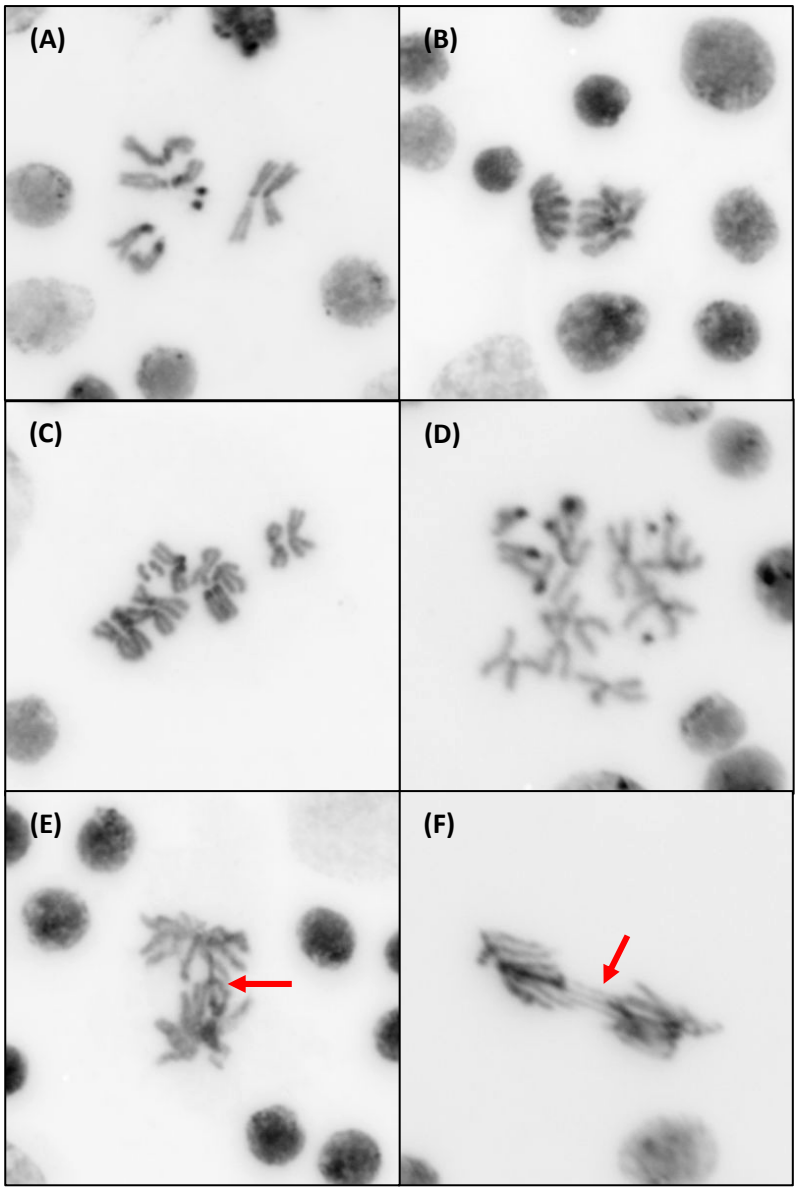

Figure 3.6: Chromosomal segregation abnormalities in neuroblast squashes. Heatshock treated hs-Gal4 (TM3, UAS-*EGFP*, *Ser*)/UAST-*Rad21*^{NC} neuroblast squashes 8 hours post-heatshock: (A) Normal diploid cell with 8 pairs of sister chromatids and (B) normal anaphase. Chromosome segregation abnormalities: (C) tetraploidy, (D) polyploidy and chromosome fragments, and (E and F) anaphases with lagging chromosomes (red arrows). (Images generated by Dr. S. Page)

3.2.5 Correction of cleavage site hypothesis

As outlined previously in section 3.2.1.2, Keall (2005) proposed the carboxy-terminal cleavage site (R474) of RAD21 was preferentially used in *Drosophila*, with seemingly minimal cleavage occurring at the amino-terminal site (R175). This is in contrast to RAD21 homologues in other species (Hauf *et al*., 1999; Uhlmann *et al*., 1999; Keall, PhD Thesis), where alteration of both RAD21 cleavage site was required before chromosome segregation inhibition was observed. The conclusion that the R474 site was the preferred site of cleavage for *Drosophila* RAD21 was based on observations that ectopic expression in the *Drosophila* eye of the amino-terminal UAST-*Rad21*^{N} mutant produced no observable phenotype. In contrast, ectopic expression of the carboxy-terminal UAST-*Rad21*^{C} mutant produced a rough-eye phenotype very similar to the phenotype produced by the "non-cleavable" mutant, with both the amino- and carboxy-terminal sites mutated (Keall, PhD thesis). Due to the apparent similarity of the GMR>*Rad21*^{C} and GMR>*Rad21*^{NC} phenotypes, it was concluded that the majority of the RAD21 cleavage must occur at the carboxy-terminal site because this mutation alone produced a phenotype equivalent to GMR>*Rad21*^{NC}. Based on this logic it was also concluded that the lack of phenotype produced by ectopic expression of *UAST-Rad21*^{C}*-GFP,* under GMR-Gal4 control, was indicative of the GFP epitope blocking functional incorporation of RAD21-GFP into cohesin rings. Consequently, further work using the GFP epitope (e.g. *UAST-Rad21*^{NC}*-GFP* transgenics) was not pursued at the time.

During the generation of the HA-tagged UAST-*Rad21* constructs, it was observed that DNA sequencing and confirmation restriction digestions indicated that the expected nucleotide substitutions were present in each construct, eye development occurred normally when ectopically expressing UAST-*Rad21*^{C}-2*HA* using GMR-Gal4. To rule out the possibility that UAST-*Rad21*^{C}-2*HA* simply failed to produce protein Western Blot analyses were performed and a protein of the correct size (120kD) was detected with anti-HA antibodies (Figure 3.5). These observations, suggested an error may have occurred in the earlier analysis of untagged UAST-*Rad21*^{C}. Combining this knowledge with previous observations of RAD21-GFP locating to chromosomes in embryos I hypothesised that GFP was not impeding functional incorporation of RAD21 and that instead pointed to the need to characterise the molecular sequences present within the *Rad21*^{C} transgenics.

The simplest explanation for the conflicting results was that a mistake had occurred during the generation of the transgenic insects. To confirm the molecular nature of the cDNAs present in the UAST-*Rad21*^{C} transgenic lines, genomic DNA was isolated from variant transgenic flies and PCR was performed on genomic DNA extracted from single flies of each genotype and using primers designed to span introns and therefore only amplify cDNA (Figure 3.1). Amplification of the amino-terminal sequence with primers DradORF and DradJ produced a 700bp DNA product, while amplification of the carboxy-terminal sequence with primers DradM and DradL produced an 850bp DNA product. The PCR products were then digested to determine the presence or absence of the *Nae*I and *Sph*I sites that were introduced during the site directed mutagenesis procedure to generate the specific R175A and RA474AG amino acid substitutions (Figure 3.7). Whilst only UAST-*Rad21*^{C} and UAST-*Rad21*^{NC} transgenic mutant lines were found to carry the carboxy-terminal cleavage site mutation (Figure 3.7), all six of the *Rad21* mutant transgenic lines were found to carry the amino-terminal R175A cleavage site mutation, including lines labelled UAST-*Rad21*^{C}. This result was confirmed for available cultures and independent UAST-*Rad21* transgenic lines (data not shown). These data demonstrated that the UAST-*Rad21*^{C} transgenics, generated and analysed by Keall (2005), carried both R175A and RA474AG amino acid substitutions and thus were in fact UAST-*Rad21*^{NC} mutants. Consequently, the hypothesis that the RAD21 carboxy-terminus cleavage site is the predominant site at which Separase cleavage occurs in *Drosophila* is no longer a justifiable claim.

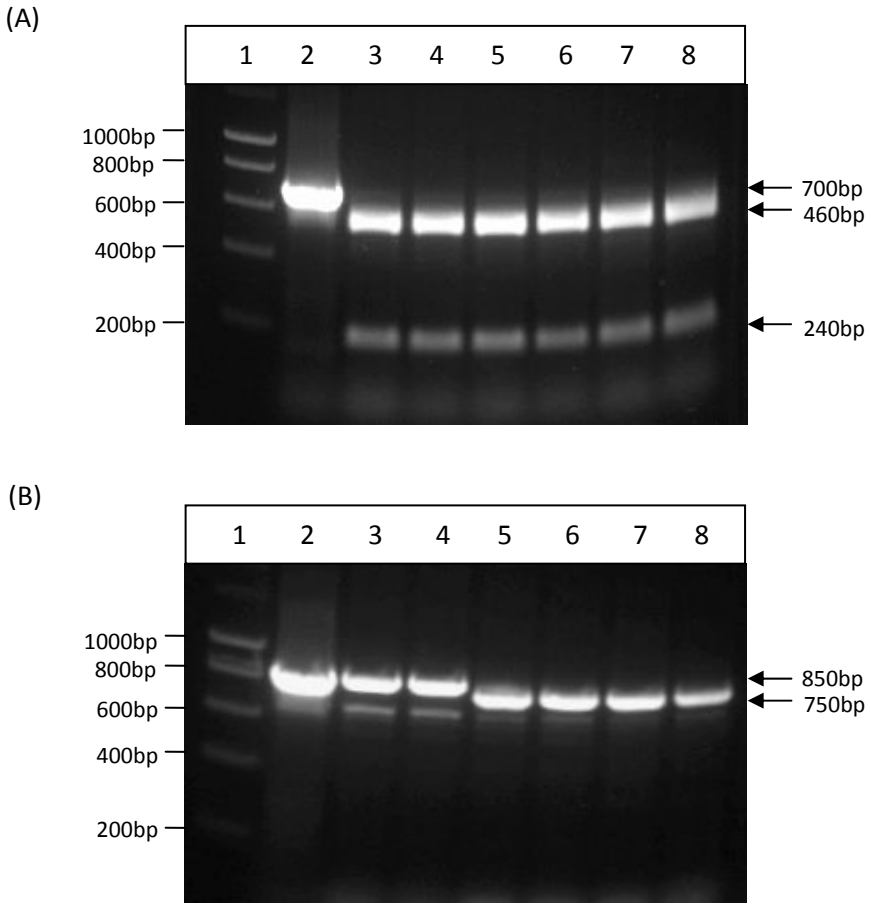

Figure 3.7: *Rad21* transgene genotyping by PCR-RFLP analysis. DNA from single-fly preparations was used as template to PCR amplify the *Rad21* cDNA present. (A) *Rad21* amino-terminal sequence digested with *Sph*I and (B) *Rad21* carboxy-terminal sequence digested with *Nae*I. The gel lanes contain: UAST-*Rad21* (lanes 2, template pUAST-$Rad21^{WT}$ plasmid construct$^{\ni}$), UAST-$Rad21^{N}$ (lanes 3 and 4, lines 4B and D2**), UAST-$Rad21^{C}$ (lanes 5 and 6, lines 1B and P11a**) and UAST-$Rad21^{NC}$ (lanes 7 and 8, lines 11B and N5**). Lanes 1 contains 0.5µg of 100bp Hyperladder (Fermentas). In gel A the presence of a single band of 700bp indicates a lack of an *Sph*I restriction site within the amplicon, while two bands of lenths 460bp and 240bp, respectively indicates the presence of the introduced *Sph*I site associated with the R175A mutation. In gel B the presence of a single band of 850bp indicates a lack of a *Nae*I restriction site within the amplicon, while the presence of a single 750bp restriction site indicates the presence of the *Nae*I restriction site a.

$^{\ni}$ The original pUAST-$Rad21^{WT}$ plasmid DNA was used as control template .

** Transgenic lines generated previously by Keall (2005).

3.2.6 Genetic influences on the Rad21^{NC} *phenotype*

3.2.6.1 Drosophila Rad21 *overexpression*

RAD21 has many functions aside from chromosome cohesion. It also has roles in apoptosis, DNA damage repair, gene expression and possibly many other as yet unrecognised functions. In an attempt to demonstrate that the RAD21^{NC} rough-eye phenotype was solely due to the introduced mutations and not a result of RAD21 overexpression, multiple copies of wildtype *Rad21-2HA* transgenes on chromosomes II and III were simultaneously expressed under the control of the GMR-Gal4 driver. No abnormal phenotype was observed from ectopic expression of one, two or three copies of *Rad21-2HA* (Figure 3.8A-C), indicating that RAD21 overproduction does not produce an observable negative effect on eye development. Additionally, when *Rad21^{NC}* and *Rad21^{WT}* transgenes were co-overexpressed under the GMR-Gal4 driver strong suppression of the rough-eye phenotype was observed (Figure 3.8F). The simplest explanation for these observations is the result of increasing the ratio of cleavable:non-cleavable RAD21 subunit and consequently decreasing the number of non-cleavable cohesin complexes present on metaphase chromosomes. Fewer non-cleavable cohesin complexes loaded onto chromosomes could reduce the strength of the chromosome segregation inhibition and thereby increase the probability of a euploid chromosome complement. The suppression of the eye phenotype through concomitant expression of a wildtype *Rad21* transgene further supports the notion that it is the altered cleavage sites and not RAD21 overexpression that is the primary cause of the GMR>*Rad21^{NC}* rough-eye phenotype. Interestingly, the introduction of a second copy of the *Rad21^{NC}* transgene only slightly enhances the rough-eye phenotype observed compared to when a single copy is expressed (Figure 3.8E).

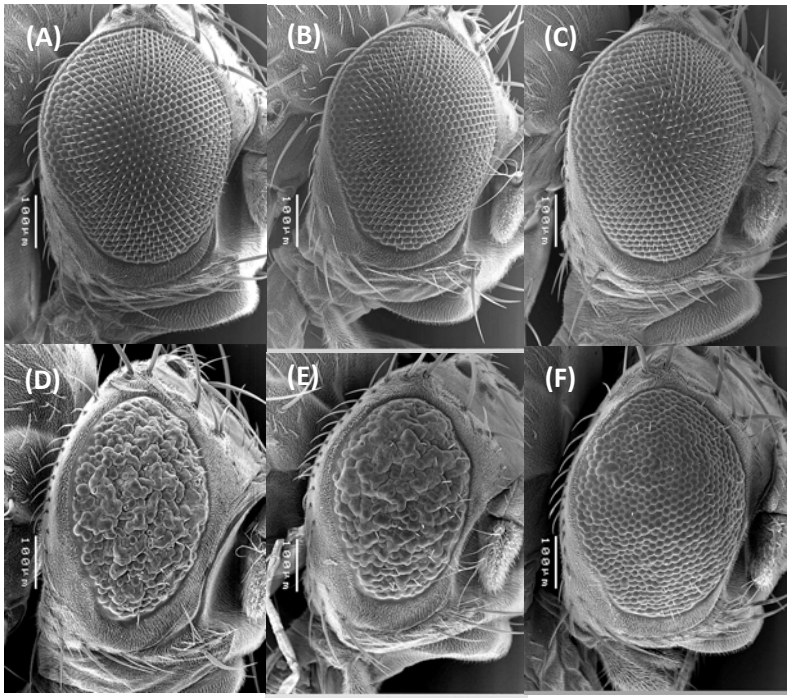

Figure 3.8: Ectopic expression of multiple copies of UAST-*Rad21* cDNAs under GMR-Gal4. (A) GMR>1x *Rad21*^{WT}-2*HA* (line 28.2), (B) GMR>2x *Rad21*^{WT}-2*HA* (line 28.2), and (C) GMR>3x *Rad21*^{WT}-2*HA* (lines 28.2 and 14.2) show no variation in eye phenotype. The GMR>*Rad21*^{NC} phenotype (line 24A, Keall, 2005) (D) is mildly enhanced by introducing a second copy of *Rad21*^{NC} (line H)(E: GMR>*Rad21*^{NC}/*Rad21*^{NC}-2*HA*) and strongly supressed by introducing a wildtype *Rad21* transgene (line 28.2) (F: GMR>*Rad21*^{NC}/ *Rad21*^{WT}-2*HA*).

3.2.6.2 The GMR driver

The eye-specific driver P{GAL4-ninaE.GMR} has been observed to affect ommatidial development in the absence of a UAS-containing transgene (Figure 3.9) (Freeman, 1996). The Gal4 system is also temperature sensitive (Duffy, 2002). Although it is not currently understood how GMR-Gal4 overexpression causes the ommatidial development effect, an increase in apoptosis has been demonstrated in the developing eye imaginal discs of both GMR-Gal4 heterozygotes and homozygotes at 25˚C and 29˚C (Kramer and Staveley, 2003). In the adult

compound eye developed at 25˚C homozygous GMR-Gal4 alone produces a distinct phenotype of gross disorganisation of the ommatidia (Figure 3.9A). Despite abnormalities being observed by Kramer and Stavely (2003) in the developing eye discs of heterozygous GMR-Gal4 larvae raised at 25˚C, the adult compound eye of heterozygous GMR-Gal4 flies has no observable abnormalities (Figure 3.9B) compared to wildtype eyes. The eyes of heterozygous GMR-Gal4 flies raised at 29˚C demonstrate a relatively mild rough-eye phenotype (Figure 3.9C). An interesting observation is that introduction of a UAST transgene almost entirely suppresses the homozygous GMR-Gal4 phenotype (Figure 3.9D). The potential for genetic modifiers to influence the GMR>*Rad21*^{NC} eye phenotype through modification of the driver alone must be kept in mind when undertaking genetic studies.

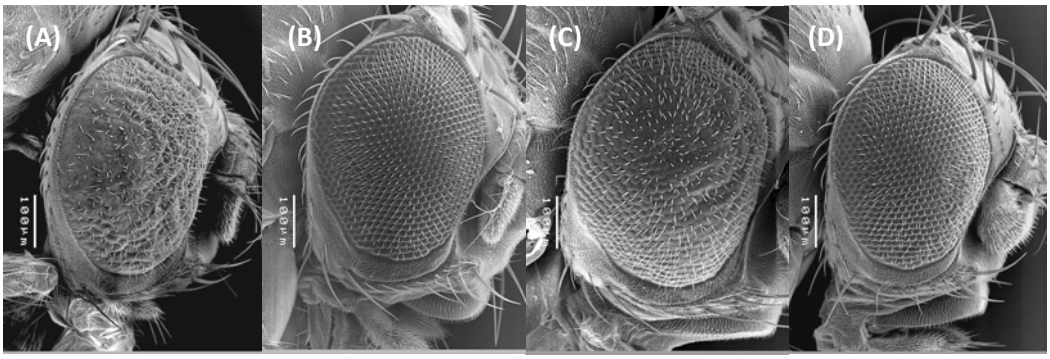

Figure 3.9: The effects of the GMR-Gal4 driver. (A) Homozygous GMR-Gal4 25˚C produces a disorganised eye phenotype with little ommatidial organisation remaining, (B) Heterozygous GMR-Gal4 25˚C produces a wildtype phenotype, (C) Heterozygous GMR-Gal4 29˚C produces a milder phenotype with some observable ommatidial orgnisation, (D) Homozygous GMR-Gal4>UAST-*Rad21*-2*HA* 25˚C produces a phenotype very close to wildtype in contrast to homozygous GMR-Gal4 alone at 25˚C.

3.2.6.3 Effects on cell survival and cell cycle

P35 is a baculovirus protein that inhibits apoptosis by blocking the activity of the apoptotic caspases -1, -2, -3, -4, -6, -7, -8 and -10 (Bump *et al*., 1995; Zhou *et al*., 1998). As demonstrated in previous studies (Keall, 2005), introduction of UAS-*p35* partially restored the size and organisation defects of GMR>*Rad21*^{NC} eye phenotype Figure 3.10). Although co-expression of p35 was observed to significantly suppress both the size and organisation defects of the GMR>*Rad21*^{NC} eye phenotype (Figure 3.10), this phenotype still demonstrates significant developmental defects compared to wildtype. Introduction of a second copy of UAS-*p35* has little effect on further suppressing the eye development defects. The work of Hay *et al*. (1994) demonstrated that p35 is capable of inhibiting almost all apoptosis, either naturally occurring or resulting from radiation induced DNA damage, consistent with the inhibition of apoptosis observed in acridine orange stained GMR>UAST-*Rad21*^{NC},UAS-*p35* (referred to from here as GMR>*Rad21*^{NC}, *p35)* eye discs from third instar larvae (Figure 3.11).

The high level of similarity between the GMR>*Rad21*^{NC}, *p35* rough-eye phenotype and the rough-eye phenotype produced when Cyclin B is overexpressed and induces slowing of the cell cycle (Okada *et al.*, 2002), led to exploration of the effects of cell cycle regulators on the GMR>*Rad21*^{NC}, *p35* phenotype. Increasing the expression of the Cyclin-dependent kinase Cdc2 was found to suppress the size and organisation of the GMR>*Rad21*^{NC}, *p35* eye phenotype, while increasing expression of Cyclin B enhances the disorganisation of the eye phenotype (Figure 3.10C-D). Cdc2 and Cyclin B are binding partners that are integral in regulating both the entry to and exit from M phase. Using phospho-histone H3 antibodies to specifically identify mitotic cells to confirm the results of Keall (2005), it was observed that there is an increase in the number of mitotic cells posterior to the morphogenetic furrow (Figure 3.12). The significant increase in mitotic cells suggests that the cleavage-resistant cohesin is slowing exit from mitosis and inducing mitotic arrest. These data are suggestive of some of the remaining disorganisation observed in the GMR>*Rad21*^{NC}*, p35* eye (Figure 3.10) being due to the slowing of the cell cycle that would occur through inhibition of chromosome segregation and further supported by modification of the GMR>*Rad21*^{NC} eye phenotype by alteration of cell cycle regulator expression levels.

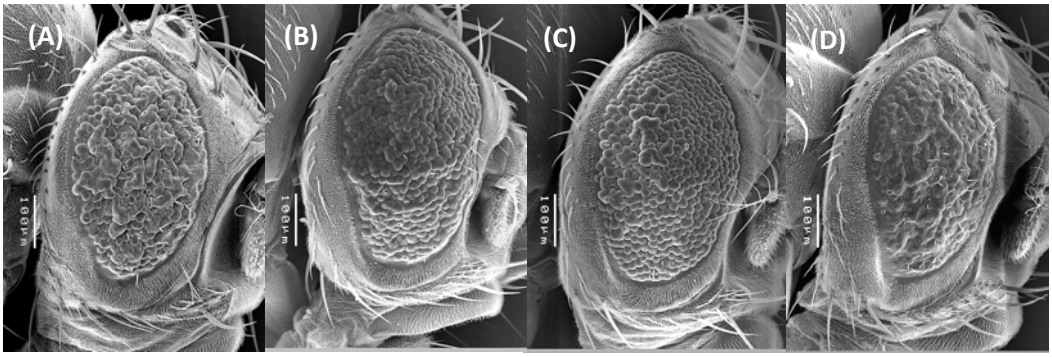

Figure 3.10: Modification of the GMR>*Rad21*^{NC} rough-eye phenotype. (A) GMR>UAST-*Rad21*^{NC}, (B) abolition of apoptosis in the GMR>UAST-*Rad21*^{NC}, UAS-*p35* transgenics results in strong suppression of the size and organisation defects, (C) GMR>UAST-*Rad21*^{NC}, UAS-*Cdc2* eyes show strong suppression of the size and organisation defects, in contrast (D) GMR>UAST-*Rad21*^{NC}, UAS-*CycB* eyes show an observable enhancement of the size and organisation defects. .

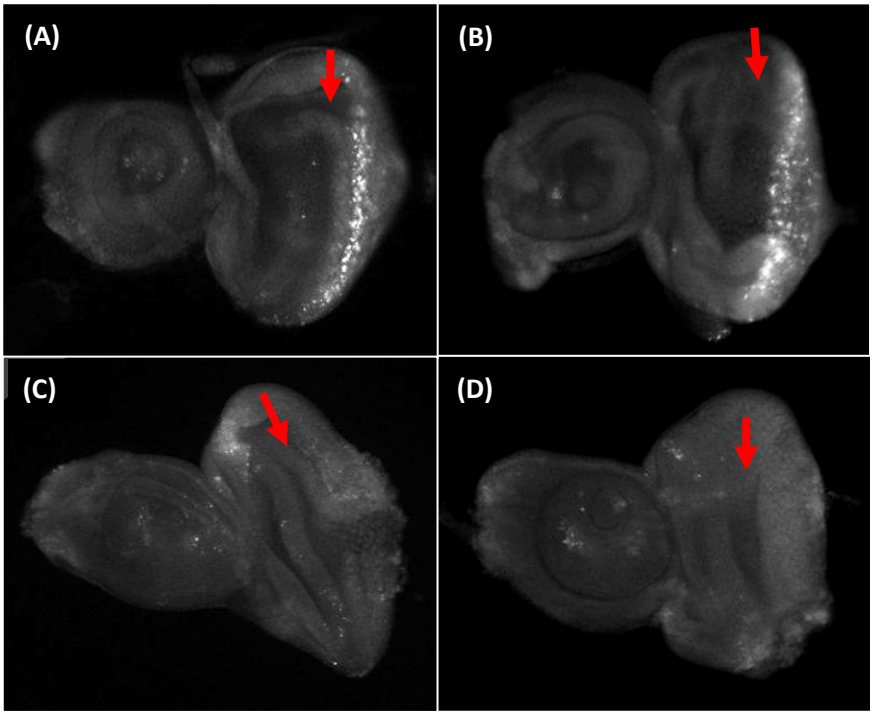

Figure 3.11: Acridine orange stained eye-antennal imaginal discs. (A) Wildtype and (B) GMR>UAST-*Rad21*^{NC} discs and (C) and (D) GMR>UAST-*Rad21*^{NC}, UAS-*p35* discs stained with acridine orange, which is specifically stains apoptosing cells. The intense acridine orange staining posterior to the morphogenetic furrow (position indicated by red arrows) in GMR>UAST-*Rad21*^{NC} discs is completely absent in the GMR>UAST-*Rad21*^{NC}, UAS-*p35* discs (bottom panels).

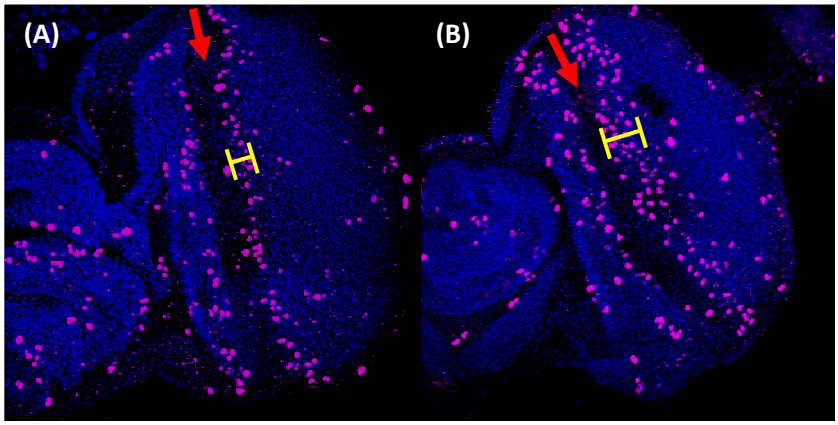

Figure 3.12: Mitotic indices of wildtype and GMR>*Rad21*^{NC} eye-antennal imaginal discs. Phospho-histone H3 antibody (magenta) and DNA (blue, To-Pro3) staining of eye discs (A) w^{1118} control and (B) GMR>UAST-*Rad21*^{NC}. The morphogenetic furrow is indicated by the red arrows and the width of the bands of mitotic cells is indicated by the yellow bars.

3.3 DISCUSSION

This study, following on from the work of Keall (2005), set out to characterise the cellular influences underlying the GMR>*Rad21*^{NC} rough-eye phenotype. To achieve this aim three main approaches were taken: (i) Generation and ectopic expression of HA and GFP epitope tagged RAD21 protein variants, (ii) Phenotypic analyses of Drosophila ectopically expressing these epitope-tagged RAD21 variants, and (iii) Biochemical analyses. From the data arising through this study and previous studies, it has been hypothesised that the GMR>*Rad21*^{NC} rough-eye phenotype results from increased cell death, reduced proliferation in the 2nd mitotic wave and perturbation of the cell cycle within the differentiating eye imaginal disc. Additionally, it was determined that RAD21 overexpression alone does not visibly contribute to the adult phenotype and that the GMR-Gal4 eye-specific driver has its own phenotype under certain conditions, which may contribute to potential genetic interactions with the GMR>*Rad21*^{NC} eye phenotype.

3.3.1 Altering the cleavage of RAD21

Ectopic expression of *Drosophila* RAD21 protein with the two putative Separase cleavage sites altered to prevent proteolytic cleavage by Separase is able to cause a severe perturbation in normal development (Keall, 2005), supporting the experimental evidence from previous studies in yeast and human cells demonstrating inhibition of chromosome segregation and resulting cellular phenotypes due to the presence of non-cleavable RAD21 (Toyoda *et al.*, 2002; Hauf *et al.*, 2001; Tomonaga *et al.*, 2000). Attempts to demonstrate an alteration of the *Drosophila* RAD21 cleavage variants using Western Blots were largely unsuccessful, most likely because of the small percentage of cleaved protein present in an asynchronous cell population at any given time. As yet the only research groups to demonstrate RAD21 cleavage products, or alteration of cleavage products through mutation, have been those working with synchronously dividing yeast and human cells (Tomonaga *et al*., 2000, Hauf *et al*., 2001).

3.3.2 Characterising the RAD21^{NC} *phenotype*

Acridine orange staining of GMR>*Rad21*^{NC} eye discs identified a large increase in the number of apoptosing cells in the wake of the morphogenetic furrow (Keall, 2005). Ectopic expression of the apoptosis inhibitor p35 under the GMR-Gal4 driver only partially suppresses the rough-eye phenotype, despite all apoptosis in the eye being inhibited (Figure 3.11). This indicates that cell death is not the only factor contributing to the reduced and disorganised eye phenotype. The most likely explanation is that although p35 may allow cells to survive the cellular catastrophe of inhibited chromosome segregation, these cells are then incapable of replicating to provide the number of cells required for normal eye development, although other cellular effects caused by viable karyotypic abnormalities cannot be discounted.

Using phospho-histone H3 staining, Keall (2005) identified an increased number of mitotic cells in the GMR>*Rad21*^{NC} eye discs following the 2nd mitotic wave progression indicating a delay in mitosis. A delay in M phase could well explain the remaining rough-eye phenotype that is not counteracted by the ectopic P35 expression as similar phenotypes have been observed in studies where a delay in S phase or M phase is induced (Xin *et al*., 2002; de Nooij and Hariharan, 1995). It is thought that this delay uncouples the cell cycle from tissue development progression and thus when the ommatidia are forming these delayed cells are not ready to be recruited to specific cell fates as normal, resulting in abnormally sized and shaped ommatidia (de Nooij and Hariharan, 1995).

The neuroblast data clearly demonstrates that the presence of cleavage resistant cohesin complexes is impeding chromosome segregation and resulting in aneuploidy and broken chromosomes (Figure 3.12). A subset of the abnormal anaphases observed appeared predominantly normal, with only a few lagging chromosomes rather than complete failure of chromosomes to separate at the onset of anaphase. The presence of tetra- and polyploid cells indicates that some cell divisions fail and this is most likely due to excessive chromatin bridges that cannot be resolved, causing a failure of the abscission required to complete cytokinesis and resulting in cytokinetic furrow regression (Steigemann *et al.,* 2009). These data demonstrate the variability of the cellular effects induced by the presence of non-cleavable cohesin complexes and likely reflects subtle variations in *Rad21*^{NC} expression. Cells with

completely normal chromosome segregation may have replicated their DNA prior to the induction of *Rad21*^{NC} expression following the heatshock treatment. Previous studies of the effects of non-cleavable *Rad21*/*Mcd1* on chromosome segregation have observed that only 10% of cells segregate chromosomes with a thick bridge of DNA lingering in the cytokinetic furrow, while the majority of cells demonstrated very thin DNA bridges linking the chromatin masses (Hauf *et al.*, 2001, Yalon *et al.*, 2004). The multiple pathways that remove cohesin from chromosomes are likely to provide significant cellular flexibility in resolving the presence of non-cleavable cohesin complexes, thereby allowing a subset of dividing cells to correctly segregate their chromosome complement.

Overexpression of RAD21^{WT} produces no observable phenotype, indicating that the rough-eye phenotype produced by RAD21^{NC} overexpression results only from alteration of the Separase cleavage sites and does not result as a consequence of an excess of RAD21 protein. This is further supported by the consistent rough-eye phenotype produced by independent transgenic lines expressing both epitope tagged and untagged RAD21 protein. Additionally, introducing an extra wildtype *Rad21* cDNA was found to strongly suppress the GMR>*Rad21*^{NC} rough-eye phenotype. This indicates that it is not the level of RAD21 protein present, but the ratio of non-cleavable cohesin complexes relative to cleavable cohesin complexes that determines the severity of the eye phenotype.

3.3.3 Altering cell cycle progression

Increased apoptosis alone is not sufficient to explain the GMR>*Rad21*^{NC} rough-eye phenotype and it is highly likely that alteration of cell cycle progression is a strong influencing factor in the final presentation of the GMR>*Rad21*^{NC} reduced and disorganised eye. Although it is vital that cell cycle events occur in a very specific order, the cell cycle is not a rigidly imposed timetable of events; instead the cell can slow or pause at particular points to allow correction of errors. When chromosome segregation is inhibited the cell cycle is able to delay cytokinesis, hence the increased mitotic index observed in GMR>*Rad21*^{NC} eye discs. This change in cell cycle progression within the developmental program of the eye can significantly affect cell differentiation, cell recruitment to specific photoreceptor differentiation

pathways and consequently lead to the perturbation of the overall organisation of the adult compound eye.

An influence on cell cycle progression by GMR>*Rad21*^{NC} is supported by an increased mitotic index in developing GMR>*Rad21*^{NC} eye discs (Figure 3.8), failure of the anti-apoptotic protein p35 to completely suppress the size and organisation phenotypes (Figure 3.7) and the modification of the eye phenotype when the cell cycle regulators Cyclin B and Cdc2 are ectopically expressed. Increased Cyclin B caused an enhancement of the size and organisation phenotypes, while increased Cdc2 caused suppression of the size and organisation phenotypes (Figure 3.7). Cyclin B degradation is required for cells to exit mitosis and so excess Cyclin B causes cells to linger in mitosis and an increase in mitotic index is observed (Okada *et al*., 2002), which would contribute to the increased disturbance of eye organisation observed. The kinase activity of the Cdc2/Cyclin B complex promotes entry into mitosis and high levels of endogenous Cyclin B expression is observed anterior to the morphogenetic furrow (Okada *et al*., 2002). As a result of the naturally high endogenous Cyclin B levels, increasing Cdc2 levels is likely to result in increased kinase activity and prompt cells to precociously entering mitosis (Marangos and Carroll, 2008). As Cyclin B regulation is more closely linked to exit of mitosis, while Cdc2 regulations is more closely linked with mitosis entry, this could explain why the binding partners have opposite effects on the severity of the eye phenotype.

Cdc2 and Cyclin B also have a critical role in regulating cohesin by inhibiting Separase activity prior to anaphase (Gorr *et al*., 2006; Holland and Taylor, 2006). Increasing Cdc2 or Cyclin B levels could also increase the negative regulation imposed on Separase and thereby result in reduced Separase activity and consequently induce enhancement of the rough-eye phenotype by further impeding chromosome separation. Enhancement is only observed when Cyclin B is ectopically expressed, while increased Cdc2 has the opposite effect of suppressing the eye phenotype (Figure 3.9), indicating that other roles for these binding partners at other times in the cell cycle may have overarching influences on the final phenotype.

3.3.4 The GMR driver

The ability of GMR-Gal4 to influence ommatidial development, independently of the presence of a UAST transgene, adds a layer of complexity to the issue, particularly as GAL4 is a yeast protein with no recognisable *Drosophila* homologue. The presence of a UAST transgene strongly suppresses the GAL4 overexpression phenotype (Figure 3.6). Along with a coding sequence of interest, a UAST transgene carries cis-acting DNA binding sites for Gal4 and frequently an eye pigmentation marker. The provision of Gal4 binding site may prevent excess Gal4 from perturbing unspecified cellular processes that result in alteration of ommatidial development. Alternatively, expression of the transgene and pigment protein marker may reduce Gal4 expression via non-specific competition for limiting transcriptional or translational factors. Mutant alleles that are able to influence Gal4 expression levels may subsequently alter GMR-Gal4 induced transgene expression.

*3.3.5 The GMR>*Rad21^{NC} *phenotype as a screening tool*

The ability of genes known to be involved in chromosome segregation to influence the RAD21^{NC} rough-eye phenotype in a predictable manner is a strong indication that this phenotype is a useful tool for performing genetic screens for modifiers of chromosome segregation. As is always the case in genetic screens, there is the potential for other factors to influence outcome of the screen. In the case of this study we have ascertained that some genes involved in apoptosis and eye development, and genes capable of influencing transgene expression levels will be able to modify the GMR>*Rad21*^{NC} eye phenotype through mechanisms other than altering chromosome segregation accuracy. These influences were kept in mind when designing experiments and analysing candidate GMR>*Rad21*^{NC} modifier loci. Particular heed was taken of wise words of Hawley and Walker (2003), "The value of whatever screen you create will be determined by the secondary screens".